The hydrodynamic short-range of the local weather forecasting

L.V. Berkovich, Yu.V. Tkacheva
Hydrometeorological Research Center of Russia
9-13 Bol'shoy Predtechenskiy Lane, 123242, Moscow-242, Russia
E-mail: lberkov@mecom.ru

A method of the hydrodynamic short-range forecast of weather [1,2] has been improved. A system coupling a basic large-scale model with a three-dimensional atmospheric boundary layer (ABL) model has been applied in the real time [3,4]. The Weather Forecasting System (WFS) operated at the Hydrometeorological Research Centre of Russia . The basic principle of the system lies in reconstruction of both synoptic-scale and mesoscale weather patterns from the output product of a large-scale prediction model by means of the ABL model algorithms and locally-adapted parameterisations: of the radiative heating effects on the near-surface air temperature variation, of a moist convection for prediction of convective precipitation as well as of some other physics . The system provides 48 h forecast of weather patterns for cities in Russia and neighbouring regions. It includes the forecast of temperature, moisture, wind, cloudiness and precipitation as well as the profiles of temperature, moisture, wind and turbulence characteristics in the lower 2-km atmospheric layer. The system of local weather forecasting, which is currently operated at the Hydrometeorological Research Center of Russia , has been developed further towards improved simulation of sharp weather changes. The goal of the system is 48 h forecasting weather elements for locations in a limited area and also for the urban and suburban areas of a longed city (like Moscow). The experience gained at its application indicates that the skill of the resulting forecasts is superior to that of the synoptic forecasts as 83 to 49 in 2002. However, proper simulation of sharp weather changes connected with significant variations in the meteorological fields calls for fine resolution in the background prediction; at the same time, the background forecast area should be sufficiently large to simulate correctly large-scale weather processes developing during 48 hours over this area.

The skill of WFS is presented here by verification statistics . The corresponding data on temperature, precipitation, and wind predictions for Moscow in 2002 are given in Table which reproduces the mean absolute forecast error of daily minimum and daily maximum temperatures ($\delta T_{\min}$, $\delta T_{\max}$; °C), 12-h precipitation amount (δP_r , mm), and wind speed (δV , m·s^{-1}).

We demonstrate the improvement of WFS forecasts over persistence (forecast error- FE and persistence error -PE).)., because there are no currently available another objective short-range weather forecasting techniques for Moscow, which we could compare our forecasts with.

	dT_{mi}	dT_{ma}	dP_r			dV			
	Projection (h)								
	0 ---	36	00-12	12-24	24-36	12	24	36	48
FE	1.7	1.9	1.0	1.1	1.4	2.0	1.8	2.1	2.0
PE	2.9	2.9	2.0	1.9	1.9	2.5	2.2	2.9	2.6

Operational forecasts calculated from operational database for Russian cities demonstrate about the same skill as shown in Table.

Further improvement to the local weather forecasting, along with development of more advanced models, calls for more complete initial observation data. In the nested fine-grid domain considered early [5], the number of currently available surface station observations is about 1-2 % of the grid-point number. Data from observations of this type are insufficient for mesoscale objective analysis, which calls for utilization of high-resolution data provided by all other available observation systems. Accordingly, data on thermophysical and dynamical characteristics of the underlying surface and on their seasonal variability with spatial resolution comparable to the model resolution are necessary. Also further developments being partly in progress now are:

- improvement of the air humidity prediction through implementation of a simplified land surface hydrology model;
- parameterized treatment of the impact of atmospheric fronts upon the evolution of meteorological variables in the boundary layer and free atmosphere; and
- development and implementation of parameterised treatment of the anthropogenic heating impacts to improve the technique of detailed weather forecasting for a large city .

REFERENCES

1. Berkovich L.V., Belousov S.L., Kalugina G.Yu, Tkacheva Yu.V. Developments in the short-term dynamical weather forecasting system at the Hydrometeorological Research Center of Russia. – Res.Act. in Atmos. And Oceanic Modeling, 1999, No.28, 5.7-5.8.
2. Berkovich L.V., Belousov S.L , Tkacheva Yu.V. Operational hydrodynamical forecasting of meteorological variables and weather patterns for locations in Russia and contiguous counties. – Russian Meteorology and Hydrology, 1998, No.4, 11-22.
3. Berkovich L.V , Tarnopolskiy A.G., Shnaidman V.A. A hydrodynamic model of the atmospheric and oceanic boundary layers. – Ibid., 1997, No.7, 30-40.
4. Belousov S.L., Berkovich L.V., V.A.Shnaydman. Short-range forecasting of meteorological variables and weather patterns. – Res.Act. in Atmos. And Oceanic Modeling, 2001, No.31, 5.1- 5.2.
5. Berkovich L.V., Belousov S.L., Kalugina G.Yu, Tkacheva Yu.V. The hydrodynamic weather forecasting for Moscow and Moscow Region.– Res.Act. in Atmos. And Oceanic Modeling, 2001, No.31, 5.3-5.4.

Arome, a new operational mesoscale NWP system for Météo-France

François Bouttier (bouttier@meteo.fr)
Centre National de Recherches Météorologiques
Toulouse, France

In an effort to improve early warnings of severe convection events, Météo-France is developing a convection-resolving data assimilation and limited area forecast model (LAM) called Arome (Applications of Research to Operations at Mesoscale). This will be used at 2 to 3km horizontal resolution over domains the size of mainland France (approx. 2000km wide) for short range predictions in replacement of the current Aladin local adaptation model (9.5km resolution today). The deadline for operational implementation is 2008. The Arome model will be coupled with Arpège, a variable-resolution global model.

Arome will reuse available software as much as possible. The software basis will be the IFS/Arpège/Aladin system developed jointly by Météo-France, ECMWF and Aladin partner countries. The dynamical core will be the so-called Aladin-NH spectral semi-implicit, semi-Lagrangian, non-hydrostatic mass-coordinate compressible model in a recent, very stable version that allows timesteps in excess of 1 minute at 2km resolution when minimal physics are used. Most of the physical parameterizations will be imported from the Méso-NH mesoscale research, and they will be different from the ones in the French global Arpège model. They will comprise: ICE3 cloud microphysics with 6 cloud and precipitation prognostic species, a version of the ECMWF FM radiation scheme, 1-D and 3-D turbulent mixing schemes with prognostic TKE, Kain-Fritsch-Bechtold subgrid-scale convection, and a PRISM/ALMA-compliant interface with externalized versions of the ISBA land surface scheme allowing e.g. CO2 flux management, variational soil moisture initialization and runoff routing for hydrological models. Advection of arbitrary passive scalar fields is provided for chemicals and aerosols, and later the Méso-NH chemical equation compiler will be included into the software. This should provide a state-of-the-art model for resolutions between 800m and 10km, with good scope for future interaction with the mesoscale research community on physics development and cloud-resolving model studies.

The main novelty will be in the data assimilation shceme. Arome being for short-range forecasting (3 to 36 hours) will run analyses using the Aladin 3D-Var-FGAT system, which is closely related with the ECMWF operational 4D-Var and 3D-Var-FGAT used in ERA-40. The obs processing will encompass all types already used in the global ECMWF and Arpège systems, with an emphasis on IR polar-orbiting sounders borne on the EOS, NPP, NPOESS and Metop platforms. Currently, ATOVS level 1C AMSU-A radiances are assimilated, with good progress being made on HIRS,

AMSU-B and AIRS. Arome will also assimilate rain radar reflectivities, conventional data with high density near the ground, and geostationary MSG/SEVIRI as radiances for clear-air humidity analysis, and as cloud analysis using pixel classification.

Current algorithmic developments include: downscaling of background error covariances, with flow-dependent vertical humidity structure functions and enhanced resolution at low level; blending of the latest large-scale 4D-Var analyses into the mesoscale 3D-Var assimilation; an accelerated version of the analysis for use in nowcasting; automated tracking of precipitation fields on radar imagery for data quality control and verification of precipitation forecasts; studies of initialization using digital filters at high resolution; optimization of the coupling between the global and mesoscale NWP systems.

Preliminary testing using data assimilation and breeding experiments suggest good potential for improving over the global-model forecasts. This is well known in cases of slow-moving convective systems. In most weather situations, the whole interior of a 2000km-wide LAM forecast will be affected by the large-scale boundary conditions within 48 hours. On the other hand, there is evidence that perturbations to the LAM initial state do affect the LAM forecast over the same range. It means that although one cannot ignore large-scale forecast errors when developing a LAM NWP system, one can still obtain good added value in the regional forecast products by investing into a sophisticated LAM model and data assimilation.

Development of a short range QPF algorithm based upon Optic Flow techniques

Neill Bowler[1*] Clive Pierce[1†]

Alan Seed[2‡]

[1]Met Office, JCHMR, Maclean Building, Crowmarsh Gifford, Wallingford, Oxon, OX10 8BB.

[2]Cooperative Research Centre for Catchment Hydrology, Weather Forecasting Group, Bureau of Meteorology Research Centre, Melbourne, Australia.

March 14, 2003

A new rain advection based nowcast scheme has been developed for GANDOLF [1, 2]. This uses optic flow ideas [3] to improve forecasting skill. The method employed removes the need to split the radar derived rain analysis into contiguous rain areas, but uses a smoothness constraint to ensure that the diagnosed velocity field varies smoothly across the analysis. The scheme has been shown to improve nowcasts of precipitation associated with cyclonic circulation around low pressure areas, and has also demonstrated superior performance during cases of embedded convection.

Optic flow methods derive from a direct application of the Optic Flow Constraint (OFC) equation. The terms in this equation are evaluated over a square block, which is considered to move with a single velocity. This velocity is found using a least squares method [4]. Block velocities are smoothed, and an instantaneous rain rate forecast is produced.

The performance of the new nowcast scheme has been compared with that of the previous GANDOLF advection scheme (not including the object-oriented conceptual life cycle model). The performance of the two schemes was compared over a period of 3 months. The new scheme showed a general improvement in forecast skill, and also demonstrated superior performance on a number of key test cases, including two precipitation events associated with severe flooding. On the basis of this evaluation the optic flow scheme has been chosen replace the previous GANDOLF advection scheme. The benefit of the new advection scheme over the previous scheme is due mainly to the difficulty in unambiguously identifying contiguous rain areas, which

*Electronic address: Neill.Bowler@metoffice.com

†Electronic address: Clive.Pierce@metoffice.com

‡Electronic address: A.Seed@bom.gov.au

is particularly troublesome on small domains, such as the UK. Thus it is concluded that block-based methods are likely to be superior to object-based methods in the majority of cases.

References

[1] N. E. Bowler and C. E. Pierce, "Development of a short range QPF algorithm based on optic flow techniques", *Met Office NWP Technical Report No. 390* (2002)

[2] N. E. Bowler, C. E. Pierce and A. Seed, "Development of a short range QPF algorithm based on optic flow techniques", *submitted to Journal of Hydrology* (2003)

[3] B. K. P. Horn and B. G. Schunck, (1981), "Determining optical flow", *Artificial Intelligence*, **17, 185-203**

[4] **A. Bab-Hadiashar and D. Suter, (1998), "Robust optic flow computation", *International Journal of Computer Vision*, 29(1), 59-77**

Predictability of Limited-Area Models: Twin and Big-Brother Experiments

Ramón de Elía * and René Laprise
Département des sciences de la Terre et de l'Atmosphère, Université du Québec à Montréal

1. Introduction

The purpose of this work is to study the predictability of limited-area models (LAMs) in an idealized context, where verification data and model errors are not an issue. Normaly, this kind of study is carried out by means of a "Twin Experiment", which consists in comparing runs of a given model initialized with slightly different initial conditions over the same domain (Anthes et al. 1985). This approach, however, does not allow to investigate the effect of the one-way nesting procedure on the predictability. The "Big-Brother Experiment" (BBE) was developed in order to analyse the effect of one-way nesting on internal variability and predictability of LAMs in a perfect-model context. It consists of a high-resolution simulation in a large domain that is considered as a reference run, and compared to other runs performed with the same model but within a smaller domain and nested in the reference simulation. The BBE, unlike to the Twin Experiment, accounts for the effect of the one-way nesting on predictability.

2. Experimental framework

The Canadian Regional Climate Model (CRCM) described in Caya and Laprise (1999) is used for a series of simulations with 45-km horizontal grid spacing, 18 levels in the vertical, and a 3-h nesting frequency. A first integration is made for a month in a domain of 196x196 grid points in the horizontal (centered in New England), nested with NCEP analyses of February 1993. This high-resolution simulation reference run becomes the "truth" to which other runs will be compared. The output fields produced by this reference run are then used to drive simulations performed over a smaller domain (100x100 in the horizontal, keeping the vertical and horizontal resolution untouched) located in the centre of the larger domain. This setup permits the comparison of the output of both simulations in the same region and therefore assesses the ability of the one-way nesting to reproduce the results of the larger domain. Since both simulations use the same formulation (dynamics, physics, resolution, numerics, etc), differences in results can be attributed unambiguously to the nesting technique.

In order to make values statistically stable, results were obtained for 24 runs of the small-domain model integrated during 4 days, each one starting on successive days of February 1993. A more detailed description of this experiment can be found in de Elia et al. (2002).

*Corresponding author address: Ramón de Elía, Groupe UQAM, Ouranos, 550 West Sherbrooke St., 19th Floor, Montréal, PQ, H3A 1B9, Canada. E-mail: relia@sca.uqam.ca

3. Differences between the Twin and the Big-Brother Experiments

a. The Twin Experiment

For the Twin Experiment the internal variability may be defined as the RMS difference between two runs started with "almost" identical initial conditions on the small domain, and it can be expressed as

$$Y_S = X_S + \epsilon_{int}, \tag{1}$$

where Y_S and X_S represent horizontal fields from two different runs of the small domain S that are function of time; X_S being considered as ground truth, and Y_S as the perturbed run. The term ϵ_{int}, the difference between these two fields, represents: $\epsilon_{int}(t=0)$ the difference in initial conditions, and $\epsilon_{int}(t>0)$ an estimation of the internal variability at subsequent times. The three terms in the expression are function of the integration time and are case dependent. The root-mean-square difference for this Twin Experiment can be expressed as

$$\mathrm{RMS}_{\mathrm{T}}^2 = \sum_D (Y_S - X_S)^2 = \sum_D \epsilon_{int}^2 = \sigma_{int}^2, \tag{2}$$

where the summation is performed over the domain D. When several cases C are available the ensemble average root-mean-square difference can be rewritten as

$$\overline{\mathrm{RMS}_{\mathrm{T}}^2} = \sum_C \sigma_{int}^2 = \overline{\sigma_{int}^2}. \tag{3}$$

The term on the right should be interpreted as the ensemble average of the spatial variance associated with the internal variability at a given integration time.

b. The Big-Brother Experiment

When the comparison of the small-domain run is carried out against the large-domain reference run, additional sources of error such us the nesting method, the nesting frequency, and the resolution in the boundary conditions should be considered. Since the internal variability cannot be separated from other sources of error, all of them are included in a single term. This can be expressed as

$$Y_S = X_L + \epsilon_W, \tag{4}$$

where the subscript S stands for small-domain run, L for large-domain reference run, and W for one-way

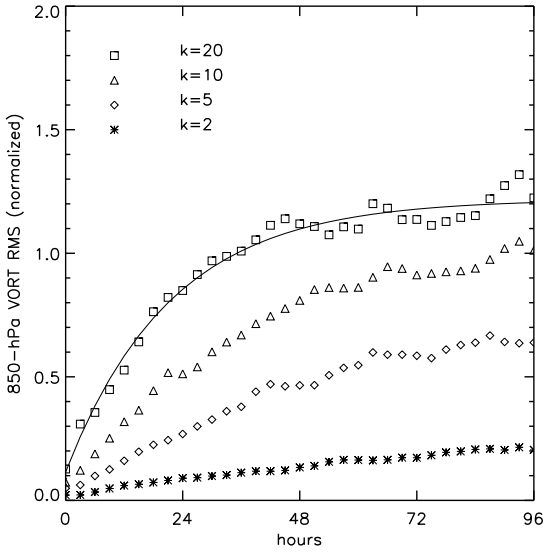

Figure 1: *Time evolution of selected wavenumbers for the normalized RMS difference for the 850-hPa vorticity fields in the BBE.*

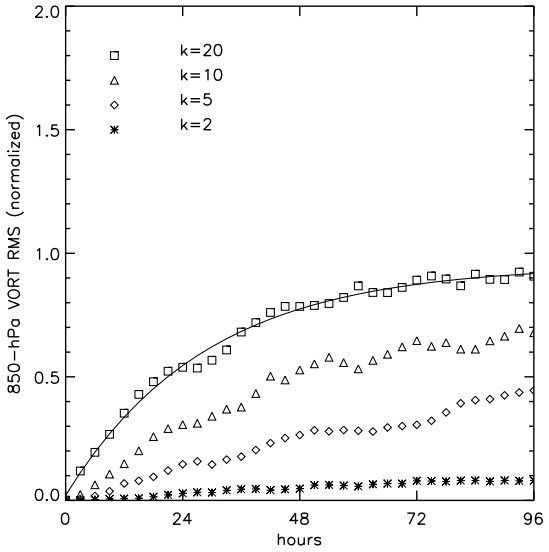

Figure 2: *Same as Fig. 1 but for the Twin Experiment.*

nesting. Following the same procedure as in the previous section the RMS of the Big-Brother Experiment can be written as

$$\overline{\mathrm{RMS}^2_{\mathrm{BB}}} = \overline{\sigma^2_W}, \tag{5}$$

where the term on the right-hand side represents the spatial variance associated with internal variability and other sources of error. Since the Big-Brother Experiment accounts for more sources of error than the Twin Experiment, this inequality must hold

$$\overline{\mathrm{RMS}^2_{\mathrm{T}}} \leq \overline{\mathrm{RMS}^2_{\mathrm{BB}}}. \tag{6}$$

In the following section, both RMS values will be estimated as a function of spatial scale with data from the simulations described in section 2.

4. Results

The difference between the 850-hPa vorticity fields of the reference run and the perturbed simulations has been decomposed spectrally, and then normalized by the average vorticity spectrum of the reference run. This normalized spectrum may be interpreted as the normalized root-mean square difference (RMS) between the fields as a function of wavenumber. Here the wavenumbers are nondimensionalised with respect to an 80-gridpoint wide domain used to do the Fourier Transform. Hence $k = 20$, for example, corresponds to a wavelength of 180 km.

The temporal evolution of selected wavenumbers is displayed in Fig. 1 for the Big-Brother Experiment. It can be seen that the error growth is highly dependent on wavenumber; being very limited for small wavenumbers and almost reaching the critical value associated with uncorrelated signals ($\sqrt{2}$) for large wavenumbers. This behavior, found in all variables studied, shows that one-way nesting mostly controls the error growth at large scales, despite the presence of all wavenumbers in the boundary conditions.

The temporal evolution of selected wavenumers for the Twin Experiment is displayed in Fig. 2. As in Fig. 1, it can be seen that growth is highly dependent on wavenumbers, being small for the large scales and large for the small scales. However, it can be seen that RMS values smaller than those of the Big-Brother Experiment are attained at all wavelengths, suggesting that the internal variability of the model does not account for the total variability observed in Fig. 1, as discussed in section 3.

5. Conclusions

Comparison of the RMS values obtained from the Big-Brother Experiment against those from the Twin Experiment indicates that the former accounts for a larger internal variability. This result suggests that measure of predictability obtained in a Twin-Experiment protocol could overerestimate its real value. For this reason, it may be convenient at the time of testing sensitivities to certain parameters in a regional model to evaluate whether a Twin or a Big-Brother Experiment are more appropriate for the interest of a particular research.

References:

Anthes et al., 1985; *Advances in Geophysics*, Vol. 28, 159-202.

Caya, D. and R. Laprise, 1999; *Mon. Wea. Rev.*,**127**, 341-362.

de Elia, R., R. Laprise, and B. Denis, 2002: *Mon. Wea. Rev.*, **130**, 2006–2023.

NCEP SHORT-RANGE ENSEMBLE FORECASTING (SREF) SYSTEM: MULTI-IC, MULTI-MODEL AND MULTI-PHYSICS APPROACH

Jun Du*, Geoff DiMego, Steve Tracton and Binbin Zhou

Environmental Modeling Center/NCEP/NOAA, Washington DC, U.S.A.

1 Current System

A prototype SREF system has been developed, implemented and run since April, 2001 at NCEP (Tracton et al., 1998; Du and Tracton, 2001). It consists of 10 members with two regional models (Eta and RSM) at 48km resolution over North America domain. Each model contributes five (5) members initiated with different perturbed initial conditions (ICs) created by the breeding method (Toth and Kalnay, 1993). It runs twice a day (09z and 21z) with a forecast length of 63 hours. Three types of SREF products, including ensemble mean/spread, spaghetti charts and probabilistic forecasts of many selected fields, are produced and displayed in real time at the following web site: http://wwwt.emc.ncep.noaa.gov/mmb/SREF/SREF.html

Preliminary results from this prototype SREF system are promising (Tracton and Du, 2001). An important lesson was also learned from our participation in the SAMEX experiment (Hou et al., 2001) during the early stage of the SREF system developement; *i.e.* perturbations in LBCs have a big impact on ensemble spread when the model computation domain is too small in size (Du and Tracton, 1999). Most of our previous reports focused mainly on multi-IC aspects. This report will, however, mainly address multi-model aspects.

2 Results from Multi-Ensemble Systems

Since both our preliminary results and the SAMEX report suggested that an ensemble system with multi models was always better than one with a single model, in terms of ensemble mean and probabilistic forecasts, a multi-model approach is one of the directions we are exploring. To continue to explore in this direction, another set of five (5) members from Eta model, but with Kain-Fritch convective scheme to replace the Betts-Miller-Janic scheme normally used by the Eta model, have been added to the 10-member SREF system to make a total of 15 members (note: strictly speaking, this step is a multi-physics rather than a multi-model approach).

Figures 1 and 2 show the September 2002 average scores of 48km ensemble median forecasts, with varying numbers of models involved, as well as the operational 12km Eta forecasts. For all six selected variables, increase in forecast accuracy of the ensemble median or mean forecasts are astonishingly significant, as the number of models increase from one model (5 members) to two models (10 members) and to three models (15 members). It's also interesting to see that the ensemble median from the 48km 5-member 1-model system performs no better than the single 12km Eta, while that from 10-member of 2-model system performs generally better than or at least comparable to the 12km Eta and that from 15-member of 3-model system outperforms the 12km Eta significantly! Similar results, but with lesser significance, can be seen for precipitation forecasts too (Fig. 3a). Figure 3b shows the improvement of probabilistic forecasts measured by Ranked Probabilistic Skill Score (RPSS) as the number of models increases.

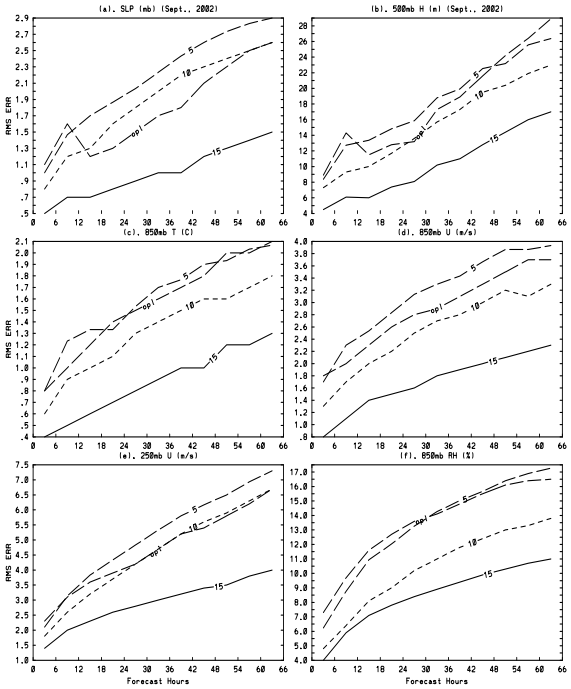

Figure 1: Sept 2002 rmse of 48km ensemble median forecasts with 1-model (averaged over "5-Eta", "5-RSM" and "5-KFeta": "5"), 2-model ("5-Eta + 5-RSM": "10") and 3-model ("5-Eta + 5-RSM + 5-KFeta": "15") SREF systems and operational 12km Eta ("opl"). Both Eta and GFS analysis are used.

One might argue that such significant improvements through a multi-model approach could stem from model bias cancellation when you combine forecasts from more than one model. Therefore, a simple technique was applied to first remove biases individually from each model and then to repeat the above calculation. It is found that the results are virtually unchanged (not shown). Of course, more study is needed to verify this. Since the ensemble size

* *Corresponding author address:* Dr. Jun Du, SAIC at Environmental Modeling Center/NCEP, 5200 Auth Road, Camp Springs, MD 20746, USA; e-mail <Jun.Du@noaa.gov>

	SREF System	out of range	expected	diff	spread
six basic fields (same as in Fig. 1)	one model (5 members)	47%	33.3%	13.7%	under dispersive
	two models (10 members)	25%	18.2%	6.8%	near perfect
	three models (15 members)	0%	12.5%	-12.5%	over dispersive
precipitation	one model (5 members)	37%	33.3%	3.7%	near perfect
	two models (10 members)	22%	18.2%	3.8%	near perfect
	three models (15 members)	15%	12.5%	2.5%	near perfect

Table 1: Average percentages of analysis not encompassed by forecasted ensemble range as measured by Talagrand distribution during September 2002.

also increases (from 5 to 15) when the number of models increases (from 1 to 3) in this study, one could argue that this big improvement resulted from the increase in ensemble size rather than in model number. However, a previous study (Du et al., 1997) shows that improvements in forecast accuracy through ensemble averaging decrease when ensemble size increases in a one-model ensemble system (multi-IC only). We therefore believe that these significant improvements (note: the improvement from 10 to 15 members was even more significant than that from 5 to 10 members!) are a result of combining multi-IC with multi-model, *i.e. multi-ensemble systems approach*!

Table 1 is a summary of the percentages where true atmosphere was beyond the range predicted by ensemble during September 2002. It can be seen that the ensemble spread is *under-dispersive* in a one-model system (5 members), but *over-dispersive* in a three-model (15 members) system. *Near-perfect spread* is seen in the precipitation forecasts.

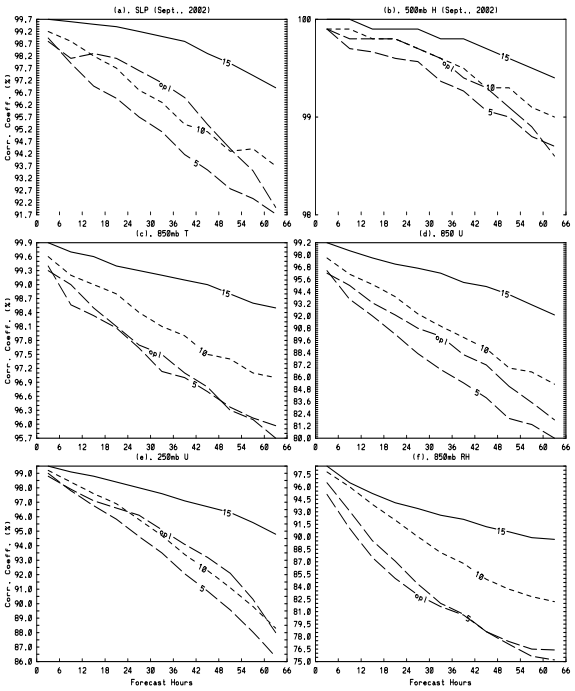

Figure 2: Same as Fig. 1 except for correlation coefficient.

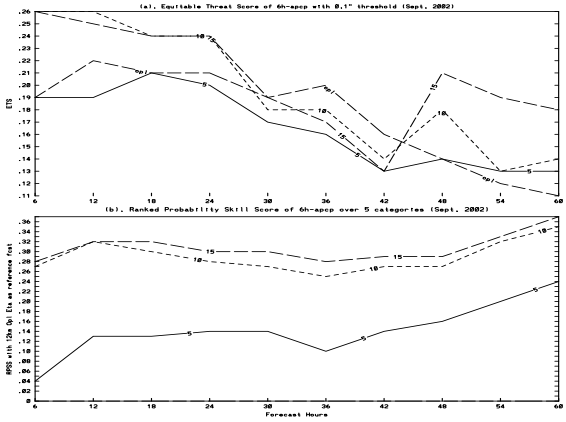

Figure 3: Same as Fig. 1 but for (a) ETS of 6h-apcp with 0.1" threshold; and (b) RPSS over five MECE categories, using 12km Eta as reference forecast. NCEP precip analysis is used in the verification.

3 Problems and Plans

Based on the positive results, NCEP SREF system will continue to be developed along the line of multi-ensemble systems. Currently, two new subsets of 5 members each with RUC and ARPS regional models respectively are being tested and will be implemented if proven to add value. Over-dispersion in spread is a possible problem in this approach that may need to be corrected.

Another problem related to this approach is that the ensemble members cluster by model in some situations. To increase the degree of freedom, given the importance of uncertainty in model physics (Stensrud et al., 2000), a new SREF system is under construction. It will address physics diversity in each model by using different alternative physics packages for a given model. Finally, the current 48km system, running twice per day, will be upgraded to 32km, running four cycles per day, in the near future.

References

Du, J., S. L. Mullen, and F. Sanders, 1997: Short-range ensemble forecasting of quantitative precipitation. *Mon. Wea. Rev.*, **125**, 2427-2459.

Du, J., and M. S. Tracton, 2001: Implementation of a real-time short-range ensemble forecasting system at NCEP: an update. Preprints, *9th Conference on Mesoscale Processes*, Ft. Lauderdale, Florida, Amer. Meteor. Soc., 355-356

Du, J., and M. S. Tracton, 1999: Impact of lateral boundary conditions on regional-model ensemble prediction. *Research activities in atmospheric and oceanic modelling* (edited by H. Ritchie), Report 28, CAS/JSC Working Group Numerical Experimentation (WGNE), WMO/TD-No., **942**, 6.7-6.8.

Hou, D., E. Kalnay, and K. K. Droegemeier, 2001: Objective verification of the SAMEX'98 ensemble forecasts. *Mon. Wea. Rev.*, **129**, 73-91.

Stensrud, D. J., J.-W. Bao, and T. T. Warner, 2000: Using initial condition and model physics perturbations in short-range ensemble simulations of mesoscale convective systems. *Mon. Wea. Rev.*, **128**, 2077-2107.

Tracton, M. S., J. Du,, 2001: Application of the NCEP/EMC short-range ensemble forecast system (SREF) to predicting extreme precipitation events. Preprints, *Symposium on Precipitation Extremes: Prediction, Impacts, and Responses*, Albuqerque, New Mexico, Amer. Meteor. Soc., 64-65.

Tracton, M. S., J. Du, Z. Toth, and H. Juang, 1998: Short-range ensemble forecasting (SREF) at NCEP/EMC. Preprints, *12th Conf. on Numerical Weather Prediction*, Phoenix, Amer. Meteor. Soc., 269-272.

Toth, Z., and Kalnay, E., 1993: Ensemble Forecasting at the NMC: The generation of perturbations. *Bull. Amer. Meteorol. Soc.*, **74**, 2317-2330.

Convective system rainfall forecast accuracy as a function of large-scale forcing

William A. Gallus, Jr. and Isidora Jankov
Dept. of Geological and Atmospheric Science, Iowa State University, Ames, IA
email: wgallus@iastate.edu

A 10 km version of the NCEP Eta model has been run over a roughly 1000×1000 km domain centered over the U.S. upper Midwest for 20 warm season mesoscale convective system cases. Simulations were performed using both the Betts-Miller-Janjic (BMJ) and Kain-Fritsch (KF) convective schemes. In addition, both schemes were used in runs initialized with several different techniques to better represent mesoscale features. These techniques included (i) an adjustment to depict cold pools, (ii) inclusion of mesonetwork surface data coupled to a deeper layer through use of the model's own vertical diffusion over a 3 hour assimilation period, and (iii) elimination of layers where relative humidity was less than 80% if radar echo was present. For all of the runs, the rainfall forecasts were examined to determine if accuracy was related to the magnitude of larger-scale forcing and thermodynamics.

To perform the analysis, five parameters (700 mb vertical motion, 200 mb divergence, 500 mb vorticity advection, 850 mb temperature advection, and surface frontogenesis) were averaged over the area within ~ 200 km of the centroid of the convective system during the first 6 hours of the simulation when organized precipitation was observed. The strongest ~ 25% of all events and weakest 25% were identified in all 5 categories. A ranking of 1 was assigned to the weakest forcings and 3 to the strongest, with 2 for the middle 50%. The rankings in all 5 categories were then summed, and the top 25% of the scores were defined to be strongly-forced events, and the lowest 25% of cases weakly-forced. For these "extreme" sets of cases (5 strongly-forced and 5 weakly-forced), average equitable threat (ET) and bias scores were determined for 6-hourly rainfall. The strongly-forced cases were represented by 12 6-hour periods of active rainfall, while the weakly-forced cases were represented by 10. Adjusted ET scores were computed using the technique of Hamill (1999) to equalize bias between the sets of cases.

In both simulations using the BMJ and KF convective schemes, strongly-forced cases earned higher ET scores (Table 1) for most rainfall thresholds. It should be noted that although the bias-equalization adjustment did change most ET scores, the changes were not large enough to affect trends shown in the table. The difference in ET scores between strongly and weakly forced cases was roughly similar when both schemes were used, except at the heaviest threshold where BMJ runs had noticeably higher ET scores for strongly-forced events, but KF runs had similar ET scores regardless of the forcing. In general, weakly forced cases with both schemes had higher biases than strongly-forced events (table not shown). For BMJ runs, the bias of the strongly-forced events was close to 1.0, so that the bias errors (overprediction of rainfall area) were worse with weakly-forced events. For KF runs, strongly-forced events generally had biases less than 1.0, and the bias error was less for the weakly-forced events.

Similar comparisons were performed for upper-level dynamic forcing (represented by 500 mb vorticity advection) and lower-level forcing (represented by surface frontogenesis). ET scores did not differ much between cases with large and small amounts of 500 mb vorticity advection. A larger difference was present when comparing strong frontogenesis cases to weak ones, especially for BMJ runs (not shown). These results may suggest that processes

typically resulting in smaller-scale, more intense upward motion, such as frontogenesis, play a greater role in influencing the accuracy of warm season convective rainfall forecasts than quasi-geostrophic forcing mechanisms such as 500 mb vorticity advection.

	Precipitation Threshold (mm)				
Model&Forcing	.254	2.54	6.35	12.7	25.4
BMJ-strong	.293	.276	.245	.180	.111
BMJ-weak	.206	.164	.138	.100	.015
KF-strong	.302	.285	.280	.185	.060
KF-weak	.216	.173	.148	.111	.067

Table 1: Adjusted ET scores (to equalize bias) averaged for strongly and weakly forced cases for simulations using the BMJ and KF schemes.

Forecast accuracy as a function of several thermodynamic parameters was also evaluated. In BMJ runs, ET scores did not vary much between cases with large and small (relative to initialization time average) convective available potential energy (CAPE). However, with KF, ET scores were much higher when CAPE was larger. For both schemes, cases with small convective inhibition (CIN) earned higher ET scores than those with large CIN for lighter rainfall thresholds, but differed little for heavier rainfall. ET scores did not differ much between cases with high and low 1000-500 mb relative humidity or precipitable water.

The impacts of the initialization adjustments as a function of large-scale forcing was also examined. The cold pool adjustment had little impact regardless of the forcing magnitude. The inclusion of mesoscale observations improved unadjusted ET scores, but primarily when forcing was strong. This result was disappointing since it was hoped weakly forced events would benefit more by having better representation of mesoscale details. The relative humidity-radar echo adjustment improved unadjusted ET scores for both strongly- and weakly-forced events when the BMJ scheme was used, but only for strong events when the KF scheme was used. With BMJ, improvement in the weakly-forced cases was comparable to that of the strong ones for light thresholds, suggesting that although mesoscale details are important in model initialization, the more positive impact occurs when the details are provided through a deep atmospheric layer. Boundary layer information alone may not help the rainfall forecast much.

In summary, we have found from a rather large sample of cases that model forecasts of warm season rainfall are more accurate when large-scale forcing is strong. The accuracy is more sensitive to low-level forcing mechanisms (such as surface frontogenesis) than forcing at upper levels (e.g., 500 mb vorticity advection). More accurate forecasts are also likely when CAPE is large, not small, if the KF scheme is used, but little difference occurs when the BMJ scheme is used. Small CIN values favor better accuracy than large values for lighter thresholds, but CIN does not strongly influence ET scores for heavier rainfall amounts.

Acknowledgments

This work was supported by NSF grant ATM-9908932 in the USWRP program, and grant ATM-0226059.

References

Hamill, T. M., 1999: Hypothesis tests for evaluating numerical precipitation forecasts. *Wea. Forecasting*, **14**, 155-167.

NWP research in Austria

T. Haiden
Central Institute for Meteorology and Geodynamics
thomas.haiden@zamg.ac.at

1. Operational forecast system

Operational limited area weather forecasts in Austria are made using version AL15 of the ARPEGE/ALADIN modelling system. ALADIN forecasts are made on two Central European domains, with horizontal resolutions of 12.1 km and 9.6 km, respectively. The number of levels in the vertical is 37 in both cases. The model is spectral, run in hydrostatic mode, with a semi-implicit, semi-Lagrangian advection scheme. Initial and boundary conditions are taken from the global model ARPEGE. A modified Bougeault scheme is used for deep convection, a first-oder closure for turbulent vertical transports, and the ISBA (Interaction Soil-Biosphere-Atmosphere) scheme is used to represent surface processes. Coupling frequency is 3 hours. Integrations up to +48 hours are performed twice a day.

2. Research

a. Numerical prediction of inversion fog and low stratus

The prediction of low-level cloudiness is a challenge for current NWP models. The underprediction of low stratus (high inversion fog) is a major forecasting problem in areas of eastern central Europe. Here the negative bias in cloud cover is the primary source of error in 2m temperature forecasts during wintertime (Greilberger and Haiden, 2003). Low stratus events are typically of large scale in the horizontal, and quasi-stationary over several days. Radiation and vertical mixing are the dominant cloud forcing mechanisms. According to 1-d and 3-d modelling studies the underprediction of inversion cloudiness is mainly due to a too smooth temperature profile across the inversion. In the case of the ALADIN model the smoothness is not caused by the limited vertical resolution but a side-effect of the specific formulation of the Richardson number dependency of the first-order turbulence scheme. This formulation sets a lower limit to vertical diffusion in the case of very stable stratification in order to avoid a reinforcing feedback loop of very cold air close to the surface. Ongoing work focuses on the development stage of the inversion, and on the comparison of first order and prognostic TKE turbulence closures in the prediction of inversion development. Also, alternative formulations for the cloudiness parameterizations have been tested (Seidl and Kann, 2002). The work is part of COST Action 722 ‘Short-Range Forecasting Methods of Fog, Visibility and Low Clouds’.

b. Deep convection triggering

On small grid scales (10 km and below) humidity convergence fields computed by a model represent not only synoptic-scale convergence but also meso-scale effects. Furthermore, one cannot expect the assumption of equilibrium between humidity convergence and convection intensity to hold on this scale. Similarly, on the small scale the triggering of convective precipitation should probably not be linked any more to the presence of humidity convergence. Convection should be allowed to become ‘active’ in the sense that it creates its

own humidity convergence. The problem of the diurnal cycle of convective precipitation, i.e. that the precipitating stage is reached too early in NWP models, is well known. Previous studies with ALADIN have shown that using a prognostic deep convection scheme tends to improve the mesoscale precipitation structures but does not solve the timing problem as long as the trigger function is kept unchanged. Simply using CAPE triggering does not solve the problem either. It appears that an improved trigger function needs to address more explicitly the cloud growth from Cu to Cu-cong into Cb. Starting in summer 2003, radar will be used to investigate the problem in more detail, and to test systematically different trigger and closure functions for deep convection.

c. Prediction of cold air pools and katabatic flows

The fact that NWP models usually employ a terrain-following coordinate system at low levels poses a problem in the forecasting of cold air pools in complex terrain. Problems also occur as aresult of the use of envelope orography, such that generally cold air pools contained within alpine basins are not simulated well. Moreover, katabatic flows, which significantly contribute to the build-up of cold air pools in mountain basins, are often too shallow to be realistically simulated in operational NWP models (Haiden and Whiteman, 2002; Zhong et al., 2002). A research initiative has been started to investigate the role of the coordinate system (terrain-following vs. z-coordinate), hydrostatic vs. nonhydrostatic simulation (Haiden, 2003b), model resolution, and turbulence parameterization on the prediction of the stable PBL in complex terrain.

d. Prediction of heavy rainfall

As a response to the August 2002 floods in Central Europe, which severely affected large parts of Austria (Haiden, 2003a), research has started on the potential of combining radar data and model results in the nowcasting of rainfall amounts for hydrological applications.

References

Greilberger, S., and T. Haiden, 2003: T2m nowcasting. *ALADIN Newsletter, 23* (in press).

Haiden, T., 2003a: On the performance of ALADIN during the August 2002 floods. *ALADIN Newsletter, 23* (in press).

Haiden, T., 2003b: A note on the pressure field in the slope wind layer. *J. Atmos. Sci.*, **60** (in press).

Haiden, T., and C. D. Whiteman, 2002: The bulk momentum budget in katabatic flow: observations and hydraulic model results. Preprints, *10th Conference on Mountain Meteorology,* Amer. Meteor. Soc., Park City, Utah, 26-29.

Seidl, H., and A. Kann, 2002: New approaches to stratus diagnosis in ALADIN. *ALADIN Newsletter, 22,* 106-108.

Zhong, S., C. D. Whiteman, and T. Haiden, 2002: How well can mesoscale models capture katabatic flows observed in a large valley? Preprints, *10th Conference on Mountain Meteorology,* Amer. Meteor. Soc., Park City, Utah, 69-72.

THE AUSTRALIAN AIR QUALITY FORECASTING SYSTEM

G. D. Hess[1], M. E. Cope[2,3], S. Lee[2], P. Manins[2], K. Puri[1], K. Tory[1], M. Burgers[4], and M. Young[5]

[1]Bureau of Meteorology Research Centre, Melbourne, Victoria, Australia, [2]CSIRO Atmospheric Research, Aspendale, Victoria, Australia, [3]CSIRO Energy Technology, North Ryde, New South Wales, Australia, [4]Environment Protection Authority of Victoria, Melbourne, Victoria, Australia, [5]New South Wales Environment Protection Authority, Lidcombe NSW, Australia. E-mail: d.hess@bom.gov.au

The Australian Air Quality Forecasting System (AAQFS) is a joint project between the Bureau of Meteorology (BoM), CSIRO Atmospheric Research (CAR), CSIRO Energy Technology (CET), the Environment Protection Authority of Victoria (EPA Victoria) and the New South Wales Environment Protection Authority (NSW EPA) to develop a high-resolution air quality forecasting system. The initial development of AAQFS was funded by the Air Pollution in Major Cities Program (sponsored by Environment Australia).

The project has a number of specific goals: to provide the ability to generate 24/36-hour air quality forecasts twice per day (available 9 am and 3 pm); provide forecasts for a range of air pollutants including oxides of nitrogen (NO_x), ozone (O_3), sulfur dioxide (SO_2), carbon monoxide (CO), benzene (C_6H_6), formaldehyde (CH_2O) and particulate matter (PM10 and PM2.5); provide forecasts at a resolution sufficient to consider suburban variations in air quality; and to provide the ability to generate simultaneous forecasts for a 'business-as-usual' emissions scenario and a 'green emissions' forecast. The latter scenario may correspond to minimal motor vehicle-usage, for example, and which could be used to indicate the reduction in population exposure that could result from a concerted public response to a forecast of poor air quality for the next day.

The AAQFS consists of five major components: a numerical weather prediction (NWP) system, an emissions inventory module (EIM), a chemical transport module (CTM) for air quality modelling, an evaluation module, and a data archiving and display module.

The BoM's operational Limited Area Prediction System (LAPS) system has been adapted for the AAQFS NWP component. Comprehensive numerics and physics packages are included and recent work has paid special attention to the resolution and treatment of surface processes. The model has 29 vertical levels and a horizontal resolution of 0.05° (covering the State of Victoria and most of New South Wales). This model is nested in LAPS at 0.375^o resolution, which in turn is nested in the BoM global model, GASP.

EPA Victoria and CSIRO, with support from NSW EPA, have developed the emissions inventory. The inventory component includes estimates of size-fractionated and speciated particle emissions, 0.01° gridded area sources over the densely populated regions and meteorologically-dependent emissions that are generated based on LAPS predictions.

The CTM has been custom-built for the project using state-of-the-art methodologies. A notable inclusion to the CTM is the Generic Reaction Set photochemical mechanism, a highly condensed (7 species and 7 reactions) photochemical transformation mechanism featuring minimal computational overhead. Parallel tests of a more comprehensive photochemistry, Carbon Bond IV, are now being conducted. Particle transformation is modelled by a sectionally-based particle scheme. The transport fields are updated every 60 minutes. The CTM has 17 vertical levels, and simulations use a 0.05° outer grid, with nested 0.01° inner grids for major urban areas.

While the focus of the AAQFS to date has been the forecasting of urban air quality, other applications are being considered. Australia is currently suffering from a prolonged drought, which has given rise to frequent dust storms. The feasibility of forecasting these dust storms is being investigated (Fig. 1). Another current activity is verifying long-range transport of the Melbourne urban plume (Fig.2).

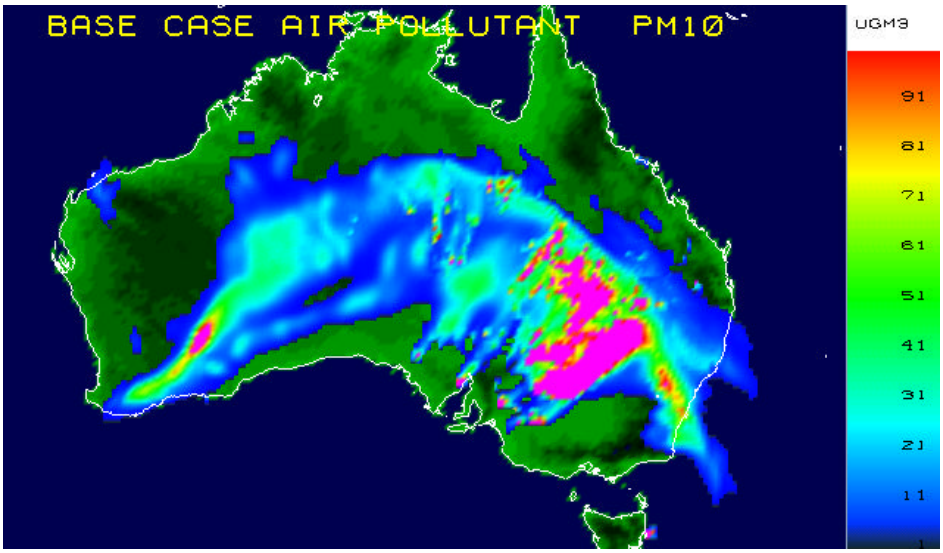

Figure 1. Simulation of a major dust storm at 1200 Australian Eastern Standard Time, 23 October 2002, which engulfed eastern cities from northern Victoria to Queensland in a deep cloud of dust. The concentrations indicate 1-hour average PM10 values.

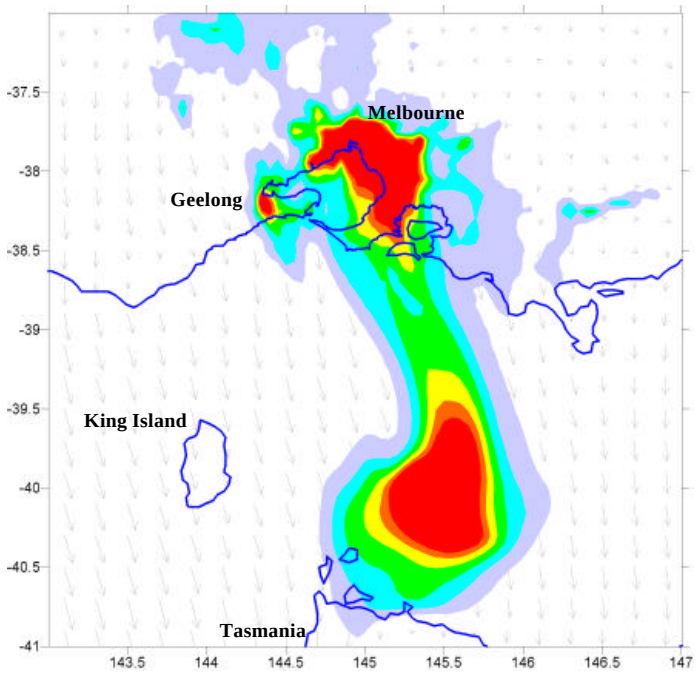

Figure 2. Simulation of the long-range transport of the carbon monoxide urban plume from the Melbourne-Geelong region to northern Tasmania at 0600 Australian Eastern Standard Time, 19 September 2001. The shaded region indicates concentrations ranging from 80–140+ ppb.

THE NCEP NONHYDROSTATIC MESOSCALE FORECASTING MODEL

Z. I. Janjic, T. L. Black, E. Rogers, H. Chuang and G. DiMego

Mesoscale Modeling Branch, Environmental Modeling Center
NOAA/NWS/National Centers for Environmental Prediction,
5200 Auth Rd., Camp Springs, MD 20746; Zavisa.Janjic@noaa.gov

Considerable experience with nonhydrostatic models has been accumulated at the scales of convective clouds and storms. However, numerical weather prediction (NWP) deals with motions over a much wider range of temporal and spatial scales. Difficulties that may not be significant or may go unnoticed at the smaller scales, may become important in NWP applications. For example, an erratic gain or loss of mass would be hard to tolerate in operational NWP applications. Another problem may arise regarding the control of spurious motions generated at upper levels by nonhydrostatic dynamics and numerics. Forcing the variables in the top layers toward a constant in time basic state in response to this problem appears to be inadequate for NWP. On the other hand, specifying time dependent computational top boundary conditions further limits the ability of the regional nonhydrostatic model to produce more accurate forecasts than the parent hydrostatic model.

Based on these considerations, a new approach has been applied in developing the NCEP Nonhydrostatic Meso Model (NMM) within the WRF effort (Janjic et al., 2001, Janjic, 2002). Namely, instead of extending the cloud models to synoptic scales, the hydrostatic approximation is relaxed in a hydrostatic model formulation. In this way the validity of the model dynamics is extended to nonhydrostatic motions, the number of prognostic equations remains the same as in the hydrostatic model, and at the same time the favorable features of the hydrostatic formulation are preserved. This approach does not involve any additional approximation.

"Isotropic" horizontal finite differencing employed in the model conserves a variety of basic and derived dynamical and quadratic quantities. Among these, the conservation of energy and enstrophy improves the accuracy of the nonlinear dynamics of the model. In the vertical, the hybrid pressure-sigma coordinate has been chosen as the primary option. The forward-backward scheme is used for horizontally propagating fast waves, and an implicit scheme is used for vertically propagating sound waves. The inexpensive Adams-Bashforth scheme is applied for non-split horizontal advection of the basic dynamical variables and for the Coriolis force. In real data runs the nonhydrostatic dynamics does not require extra computational boundary conditions at the top.

The computational cost of the nonhydrostatic extension is about 20% of the cost of the hydrostatic dynamics, both in terms of computer time and memory. The relatively low cost of the nonhydrostatic dynamics justifies its application even at medium resolutions.

In high resolution NWP applications, the efficiency of the described computational algorithm significantly exceeds those of several established state-of-the-art nonhydrostatic models. It is argued that the high computational efficiency has been achieved primarily due to the design of the time-stepping procedure. The high computational efficiency of the model demonstrates that meaningful nonhydrostatic forecasting/simulations are rapidly becoming feasible at smaller centers also, using workstations and PC's.

The dynamical core of the NMM has been adopted as one of the three major alternative dynamical cores within the WRF model. The conversion of the NMM code to the WRF standards and its incorporation into the WRF modeling infrastructure are nearing completion.

The NMM has been run operationally at NCEP (Black et al., 2002). In high resolution NWP applications, the model has been highly competitive with mature hydrostatic NWP models and with other nonhydrostatic models. The 42 hour forecasts of 10 m wind in Southern California, valid February 6, 2003, 00 UTC, obtained using the operational hydrostatic 12 km Eta model (left panel) and the 8 km NMM (right panel) are shown in Fig. 1. The heavy arrows represent the observed winds. As can be seen from the plots,

the NMM forecast agrees much better with the observations than does the Eta forecast. Further examples of the NMM forecasts can be found in Black et al. (2002).

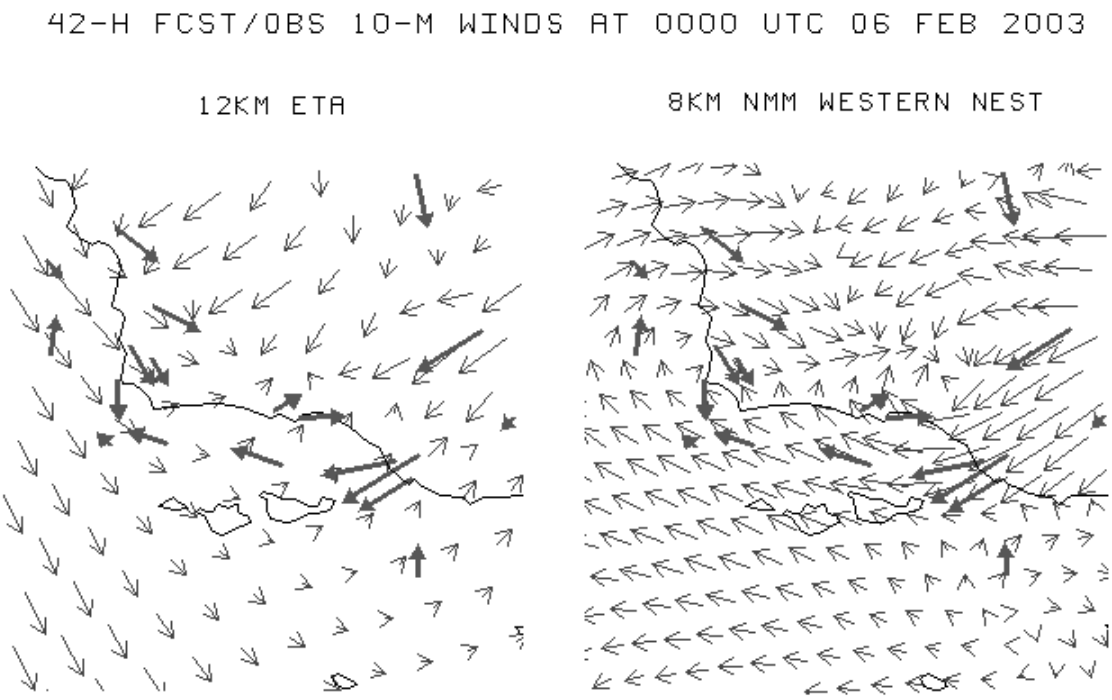

Fig. 1. The 42 hour forecasts of 10 m wind in Southern California valid February 6, 2003, 00 UTC obtained using the operational hydrostatic 12 km Eta model (left panel) and the 8 km NMM (right panel). The heavy arrows represent the observed winds.

REFERENCES

Black, T., E. Rogers, Z. Janjic, H. Chuang, and G. DiMego, 2002: Forecast guidance from NCEP's high resolution nonhydrostatic mesoscale model. Preprints 15th Conference on Numerical Weather Prediction, San Antonio, TX, Amer. Meteor. Soc., J23-J24.

Janjic Z. I., J. P. Gerrity, Jr. and S. Nickovic, 2001: An Alternative Approach to Nonhydrostatic Modeling. *Monthly Weather Review*, Vol. **129**, 1164-1178.

Janjic, Z. I., 2002: A Nonhydrostatic Model Based on a New Approach. *Meteorology and Atmospheric Physics,* DOI 10.1007/s00703-001-0587-6.

Convective Asymmetries Associated with Tropical Cyclone Landfall Part I: F-Plane Simulations

Xudong Liang*[1] [2]and Johnny C L Chan [2]

[1] *Shanghai Typhoon Institute, China Meteorological Administration*
[2]*Laboratory for Atmospheric Research, Department of Physics and Materials Science City University of Hong Kong*
*Email: liangxd@mail.typhoon.gov.cn

1. Introduction

The problem of tropical cyclone (TC) landfall has received more attention in recent years especially after it has been listed as one of the foci of the US Weather Research Program. The earlier modeling efforts by Ooyama (1969), Rosenthal (1971), Tuleya and Kurihara (1978) and Tuleya et al. (1984) have given some characters of the landfall TC. This study therefore represents an attempt to investigate the physical processes that, under idealized conditions, lead to changes in the rainfall distribution in a TC prior to, during and after landfall using the mesoscale model MM5. The following experiments on *f* plane and without mean-flow are performed: turning off the sensible heat flux over land (Expt. 2), turning off the moisture flux over land (Expt. 3), and setting the roughness length to be 0.25 m over land (Expt. 4). The coastline is moved to represent the movement TCs In all of the experiments.

2. Results

The results of the experiments suggested that cutting off the moisture flux over land should have a profound effect on the TC characteristics while changing the sensible heat flux has very little impact. In Expt.3, before and during TC landfall, the maximum rainfall primarily occurs in upper and upper left quadrants (Fig. 1), which are very similar to that in Expt.4. Because the change in the roughness length of the underlying surface in Expt.4 causes a change in the wind speed in the PBL, which will then reduce the moisture flux. Therefore, both in Expt.3 and 4, the moisture flux on the land surface is smaller than that on the sea surface. These results also suggest that the moisture flux is very important to determine the rainfall pattern before and during TC landfall, and the convergence/divergence in the onshore/offshore areas may not play the key role in determining the distribution of precipitation.

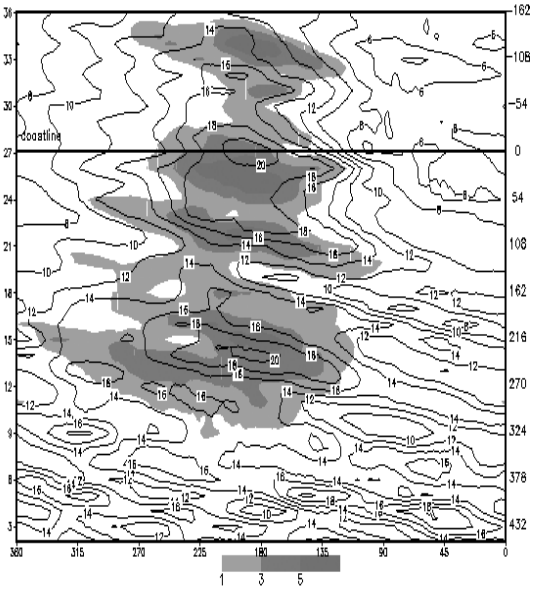

Fig. 1 Azimuthally-summed 1-h rainfall (cm) from 1 to 36 h in Expt. 3. Shaded is the increased rainfall compared with the control run. The 1-h rainfall is obtained by radially summing the hourly rainfall within each 15-km, 1 degree azimuth box (centered on the TC center) out to 300 km at each degree from east. The x-axis is the degree relative to east (anti-clockwise, 1^{o}), left ordinate is the integrating time and right ordinate is the distance of the TC center relative to the coastline in km.

3. Effect of moisture flux

During TC landfall, moisture flux over land is less than that on the sea, but it is not always favorable to reduce the rainfall. In fact, it usually increases the rainfall in upper and upper left quadrants related to the TC and reduces it behind. The reason is that the dry air over land and moist air over the sea are advected into the inner area of the TC and raised by rising motion. As a result, the instability should be decreased/increased by the inflow of dry/moist air in lower levels with moist/dry air in upper levels. The asymmetric distributions of $\partial\theta_{se}/\partial z$ in Expt. 3 (Fig. 2) indicate that the lower levels in inner areas to the east and north of TC center are more unstable than those to the west and south while to the east and north are more stable in the higher levels before landfall. The increased/decreased instability will lead to increase/decrease of upward motion. Therefore, the anomalous upward motion begins to the east and north of TC at lower levels and increases to the west and south at high levels before and during landfall. The rainfall anomaly caused by upward motion does not directly occur in the east and north, because the rainfall occurs only after the air is raised up to a certain height. For a TC, the average horizontal wind speed is very large; when the air is rising, it is cyclonically advected to the downstream areas so that enhanced rainfall exists from northwest to southwest of the TC due to the anomalous upward motion.

References

Tuleya R. E. and Y. Kurihara, 1978: A numerical simulation of tropical cyclones. *J. Atmos. Sci.*, **35,** 242-257.

Tuleya R. E., M. A. Bender and Y. Kurihara, 1984: A simulation study of the landfall of tropical cyclones using a movable nested-mesh model. *Mon. Wea. Rev,* **112,** 124-136.

Ooyama, K., 1969: Numerical simulation of the life cycle of tropical cyclones. *J. Atmos. Sci.*, **26,** 3-40.

Rosenthal, S., 1971: The response of a tropical cyclone model to variations in boundary layer parameters, initial conditions, lateral boundary conditions and domain size. *Mon. Wea. Rev*, **99,** 767-777.

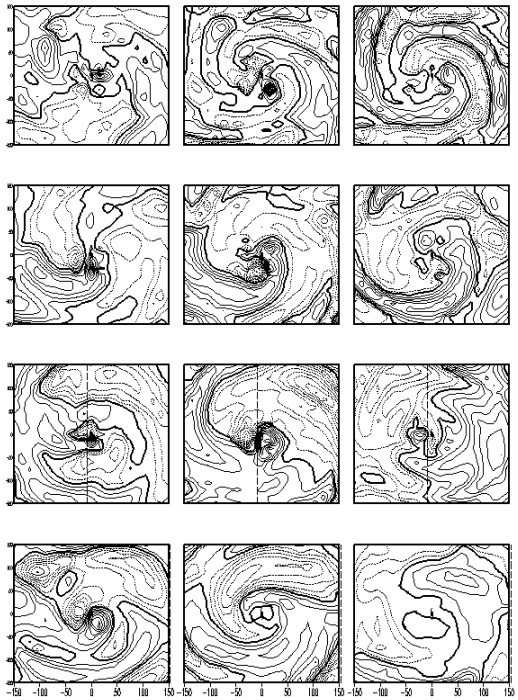

Fig. 2. Anomalies of $\partial\theta_{se}/\partial z$ (unit: K km^{-1}) at σ levels 3 (~ 920 hPa), 5 (~ 850 hPa) and 7 (~ 750 hPa) (from left column to right) in Expt. 3 at 9, 18, 27 and 36 h (from top row to bottom). The abscissa and ordinate are respectively the zonal and meridional distances (km) relative to the TC center, which is represented by the typhoon symbol. The straight long dashed line indicates the coastline.

DEVELOPMENT OF A TWO-WAY MULTIPLY-NESTED MOVABLE MESH TYPHOON MODEL USING THE CLOUD RESOLVING NONHYDROSTATIC MODEL

W. Mashiko and C. Muroi
Meteorological Research Institute, JMA, 1-1 Nagamine, Tsukuba, Ibaraki 305-0052, Japan
(corresponding author : wmashiko@mri-jma.go.jp)

1. Introduction

In order to get better prediction of typhoon track, intensity, heavy rainfall and strong wind distribution, and inner structure, we are on the way to develop a two-way multiply-nested movable mesh typhoon model based on Meteorological Research Institute/Numerical Prediction Division unified nonhydrostatic model of the Japan Meteorological Agency (MRI/NPD-NHM; Saito et al., 2001).

MRI/NPD-NHM has been used to simulate various cases of mesoscale phenomena. However, numerical experiments of typhoon in high resolution have rarely been conducted due to the limited computer resources.

For the precise prediction of typhoon, enormous computer resources are needed because environment fields around a typhoon largely affect the typhoon evolution and therefore a large model domain is needed. Moreover, since convective processes play an important role in the typhoon dynamics, fine mesh (horizontal grid size; less than 1-2km) that represents convection is desirable especially near the typhoon center.

The major advantage of the two-way nested model is that it can effectively reduce computational time and memory requirements because both the large domain and high resolution can be accomplished together by arranging fine mesh over the typhoon area and coarse mesh over the environment.

2. Model description

The main procedures of the two-way interactive mesh refinement scheme are (1)construction of an interface between coarse mesh and fine mesh, (2)interpolation that is used to provide initial and boundary values of fine mesh, (3)feedback from fine mesh to coarse mesh, and (4)boundaries conditions for fine mesh.

We employed monotone advection algorithms for the interpolation procedure(2) and one point feedback with a smoother–desmoother used in Penn State/NCAR Mesoscale Model (Grell et al., 1995) for the feedback procedure(3). As for boundaries conditions(4), we adopted the radiative-nesting boundary conditions considering the difference between coarse and fine mesh's values (Chen 1991). Some Fortran90 modules concerning two-way nesting were added to MRI/NPD-NHM in such a way that minimizes the change of its original source code.

3. Basic verification against 3-D mountain waves

To check the dynamical core of the model, we performed three-dimensional numerical simulations of a mountain flow with the model. The two-way nested model that covers the near-mountain area with fine mesh and elsewhere with coarse mesh produced almost the same results as those from the model with fine mesh all over the model domain and no erroneous wave reflection occurred near the boundaries (Fig.1). And computational time and memory could be reduced, compared with the model covered with all area fine mesh.

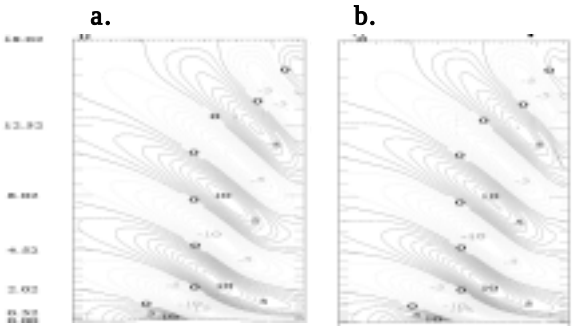

Fig.1 Vertical cross section of vertical wind through mountain top at 2-hour
a. all area fine mesh (magnified corresponding to 2-way fine mesh area) **b.** fine mesh (2way)

4. Numerical experiment of Typhoon Saomai

Numerical experiment of Typhoon Saomai (2000) was conducted with the two-way double-nested movable mesh model. The model is nested with the Regional Spectral Model (RSM : horizontal resolution about 20km), an operational hydrostatic model of JMA. The initial condition is also supplied from RSM. The coarse mesh contains 200x200 grid points horizontally (grid size 18km), which covers a domain of $(3600km)^2$ shown in Fig.3. The squares in Fig.3 show the domain of the fine mesh (horizontal grid size 6km : 151x151), which moves with the typhoon. Further descriptions of the model and nesting procedure are given in Table1 and Fig.2, respectively. Cold-rain explicit cloud microphysics were employed and convective adjustment parameterization is used jointly only in the coarse mesh. Fig.4 compares the central pressure of the model storm with the best track one determined by the RSMC-Tokyo. Fig.5 shows the sea-level pressure field and hourly accumulated rainfall of fine mesh at 34 hour forecast. As a whole, the model reproduced not only typhoon intensity but also rain distribution and the scale of eye well.

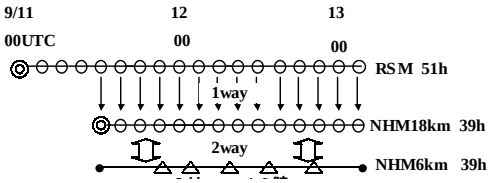

Fig.2 Relationship of nesting between numerical models
△ shows the timing of fine mesh's movement

Table1. The model design

Domain	Coarse mesh	Fine mesh
Dimension (x,y)	200x200	151x151
Area coverage (km^2)	3600x3600	906x906
Vertical levels	38	38
Grid size (km)	18	6
Time step (s)	30	15

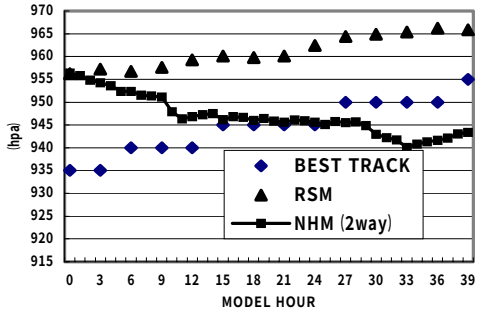

Fig.4 Time series of the minimum central pressure of Typhoon Saomai

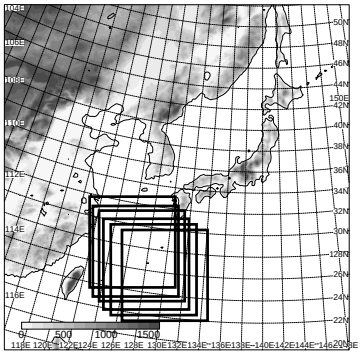

Fig.3 Orography of coarse mesh and domain of fine mesh

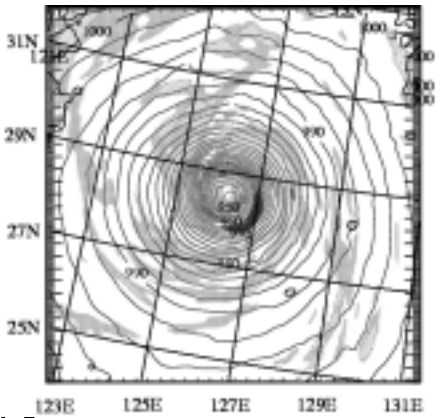

Fig5. Sea-level pressure and hourly rainfall at 34-hour forecast of fine mesh (22UTC 12Sep) Contour interval is 2hpa. The interval of hatch is 0.1,1,10,20mm.

5. Future plan

We are planning to conduct further high resolution experiments near typhoon center with triple-nested model in order to resolve the details of inner structure. Moreover, we'll examine the effect of two-way nesting.

References

C.Chen : A Nested Grid, Nonhydrostatic, Elastic Model Using a Terrain-following Coordinate Transformation The Radiative-nesting Boundary Conditions. Mon.Wea.Rev119(1991) 2852-2869

G.A.Grell, J Dudhia, D.R.Stauffer : A Description of the Fifth-Generation Penn State/NCAR Mesoscale Model(MM5). NCAR TECHNICAL NOTE (1995) 122p

Saito, K., T. Kato, H. Eito and C. Muroi, 2001 : Documentation of the Meteorological Research Institute/Numerical Prediction Division unified nonhydrostatic model. Tech. Rep. MRI, 42

THE LIMITED–AREA ENSEMBLE PREDICTION SYSTEM COSMO–LEPS

T. Paccagnella, D. Cesari, C. Marsigli, A. Montani, F. Nerozzi and S. Tibaldi

ARPA–SMR, Regional Meteorological Service, Bologna, Italy
corresponding author: cmarsigli@smr.arpa.emr.it

The forecast of localised and severe weather events is still a challenging problem. The key role played by mesoscale and orographic–related processes can seriously limit the predictability of intense and localised events. Although the use of high–resolution limited–area models (LAMs) has improved the short–range prediction of locally intense events, it is sometimes difficult to forecast accurately their space–time evolution for ranges longer than 48 hours. Thanks to ensemble prediction systems (EPSs), many weather centres, and ECMWF among them, have given more and more emphasis to the probabilistic approach. Regarding the use of limited–area models within ensemble systems, ARPA-SMR developed LEPS, a Limited–area Ensemble Prediction System. Out of a "super–ensemble" of 153 elements of three consecutive operational ECMWF EPS runs, five clusters are identified and, for each of them, a cluster representative member (RM) is chosen. Each of such RMs provides both initial and boundary conditions for a LAM integration, generating in this way a small–size, high–resolution ensemble. The LEPS methodology allows to combine the benefits of the probabilistic approach (a set of different evolution scenarios is provided to the forecaster) with the high–resolution detail of the LAM integrations, with a limited computational investment (Marsigli et al., 2001, *Quart. J. Roy. Meteor. Soc.*, **127**, 2095–2115; Molteni et al., 2001, *Quart. J. Roy. Meteor. Soc.*, **127**, 2069–2094; Montani et al., 2001, *Nonlin. Proc. Geophys.*, **8**, 387–399). In the quoted references it has been shown that, over a number of test cases and for several forecast ranges (48–120 hours), LEPS performs better than EPS concerning the quantitative forecast of intense precipitation, as well as the geographical localisation of the regions most likely affected by the events. Following the encouraging results of an early experimental phase, the generation of an "experimental–operational" limited–area ensemble prediction system, the COSMO–LEPS project, has recently started on the ECMWF computer system under the auspices of COSMO. COSMO (COnsortium for Small–scale MOdelling, www.cosmo–model.org) is a consortium involving Germany, Italy, Switzerland, Greece and Poland on the developement of the limited–area non–hydrostatic model Lokal Modell (LM). COSMO–LEPS aims therefore at the development and pre–operational test of a "short to medium–range" (48–120 hours) probabilistic forecasting system using a LAM over a comparatively large domain (see fig. 1), covering all countries involved in COSMO. Thanks

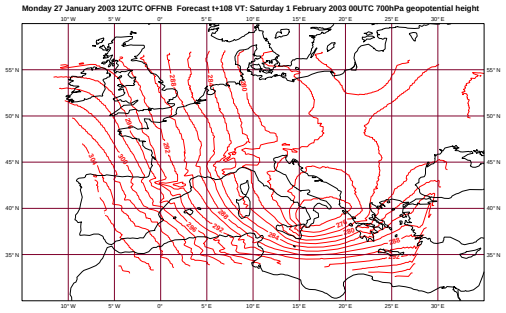

Figure 1: Operational COSMO–LEPS domain.

to the experience gained during the early experimental phase, it was decided to set–up the suite as follows:

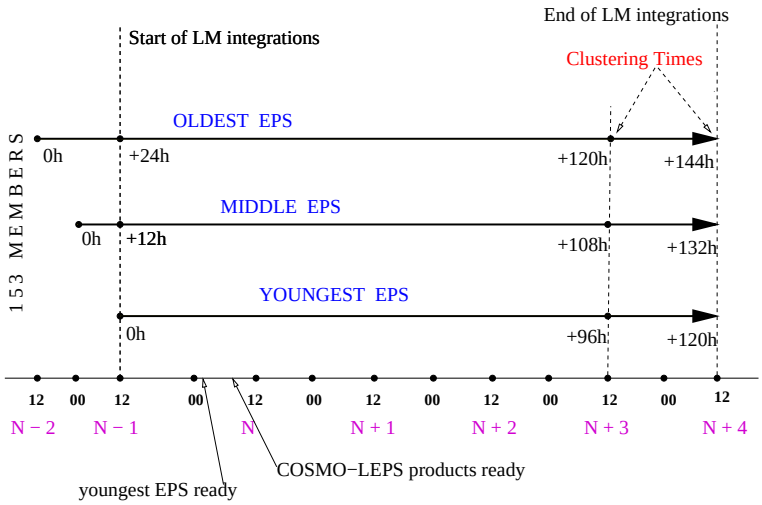

Figure 2: Details of COSMO–LEPS suite.

- three successive 12–hour–lagged EPS runs (started at 12 UTC of day *N–2*, at 00 and 12 UTC of day *N–1*) are grouped together so as to generate a 153–member super–ensemble; (see fig. 2);
- a hierarchical cluster analysis is performed on the 153 members so as to group all elements into 5 clusters (of different populations); the clustering variables are Z, U, V and Q (specific humidity) at three pressure levels (500, 700, 850 hPa) and at two forecast times (fc+96 and fc+120 for the "youngest" EPS); the cluster domain covers the region 30N–60N, 20W–40E;
- within each cluster, one representative member (RM) is selected according to the following criteria: the RM is that element closest to the members of its own clusters and most distant from the members of the other clusters; distances are calculated using the same variables and the same metric used in the cluster analysis; hence, 5 RMs are selected;
- each RM provides initial and boundary conditions for the integrations with LM, which is run 5 times for 120 hours, always starting at 12UTC of day *N–1* and ending at 12UTC of day $N + 4$;
- the LM has a horizontal resolution $\Delta x \simeq 10$ km, 32 vertical levels and the time–step used for the integrations is 60 sec;
- probability maps based on LM runs are generated by assigning to each LM integration a weight proportional to the population of the cluster from which the RM (providing initial and boundary conditions) was selected; deterministic products (that is, the 5 LM scenarios in terms of surface and upper–level fields) are also produced;
- LM grib–files are disseminated to the COSMO community for evaluation;

COSMO–LEPS products are usually available by 9UTC of day *N*, well in time to be evaluated by operational forecasters. COSMO–LEPS dissemination started during November 2002 and, at the time of writing (March 2003), the system is still being tested to assess its usefulness in met–ops rooms, particularly in terms of the assistance given to forecasters in cases of extreme events. An objective probabilistic verification of the system is also being carried on.

Analysis of the evolution and motion of tropical cyclones on the basis of calculations using the ETA model and satellite data

(Section 5)

A.E.Pokhil, A.D.Naumov

Moscow, Hydrometeorological Research Center of Russia
9-11 Bolshoy Predtechenski Lane, 123242 Moskow,Russia. E-mail: pokhil@mecom.ru
and anaumov@mecom.ru

It has been investigated whether it is possible to take into account multiple interaction of tropical cyclones in the forecast of their motion in the north-west of the Pacific based on calculations of pressure fields and the wind using the ETA model and the comparison of the calculation results with the GMS satellite data and actual TC trajectories. The performed analysis of the behavior of the interacting TCs has revealed, in particular, strange motion of the vortices and their sudden disappearance. In the typhoon season of this year two TC pairs, which interacted during definite time intervals, were of particular interest for investigation. These were Chataan and Nakri (9 - 10 July); Halong and Nakri (12 - 14 July). In the first case Chataan was the leading one. The distance at which their interaction became detectable was 1000 km. It is well seen at the fields calculated using the ETA model (Fig. 1a). Simultaneously Chataan breaks in two vortices, its south part keeps interacting with Nakri: on 10 July the trajectory of Nakri sharply changes its direction, and the TC moves right the east towards the newly formed vortex. On 11 - 12 July they merge into a single vortex, which can be easily seen from the satellite data. On 13 July at midday the distance between the centers of the approached by that moment TC Halong and Nakri constitutes 800 - 900 km. Intensive interaction is observed, with the stronger typhoon Halong entrapping Nakri and the last one ceasing to exist as a separate formation (Fig. 1b). Further motion of the typhoon takes place with a 90° turn. Having turned the TC moves along the polar front in the north-east direction.

The calculation of the wind and pressure fields using the ETA model reflects rather well the location of strong formations (STS and Ty), whereas weak vortices are not distinctly detectable in the analysis of fields. Besides that, the pressure in the center of vortices is not consistent with actual pressure. As far as the character of the vortex interaction is concerned, it depends to a considerable extent on the parameters of the vortices themselves. It has been shown in our previous works devoted to the experiments with vortex pairs using barotropic and baroclinic models /1, 2, 3/. So, to obtain good calculation results, it is necessary to synthesize the algorithm of the restoration of the initial vortex, which models the TCs in the fields of objective analysis (“vortex initialization”).

For understanding the evolution of vortices and their interaction the comparison of calculations with the satellite data is quite useful.

References

1. A.E.Pokhil, A.V.Nikolaeva. The behavior of a pair of interacting cyclonic vortices in the barotropic model of the atmosphere. Meteorology and Hydrology., 2000, No. 11.
2. Pokhil A.E., Sitnikov I.G.Diagnostics of motion and development of two series of tropical cyclones for the 2000 typhoon season. -CAS/JSC Working Group on numerical experimentation. Research activities in atmospheric and oceanic modelling. Report N 31, april 2001. WMO/TD-N 1064.
3. A.E.Pokhil, A.V.Nikolaeva. Numerical experiments with a pair of interacting vortices in a baroclinic model. Meteorology and Hydrology, 2002, No. 3.

Sea level pressure, wind 1000 hPa

a)

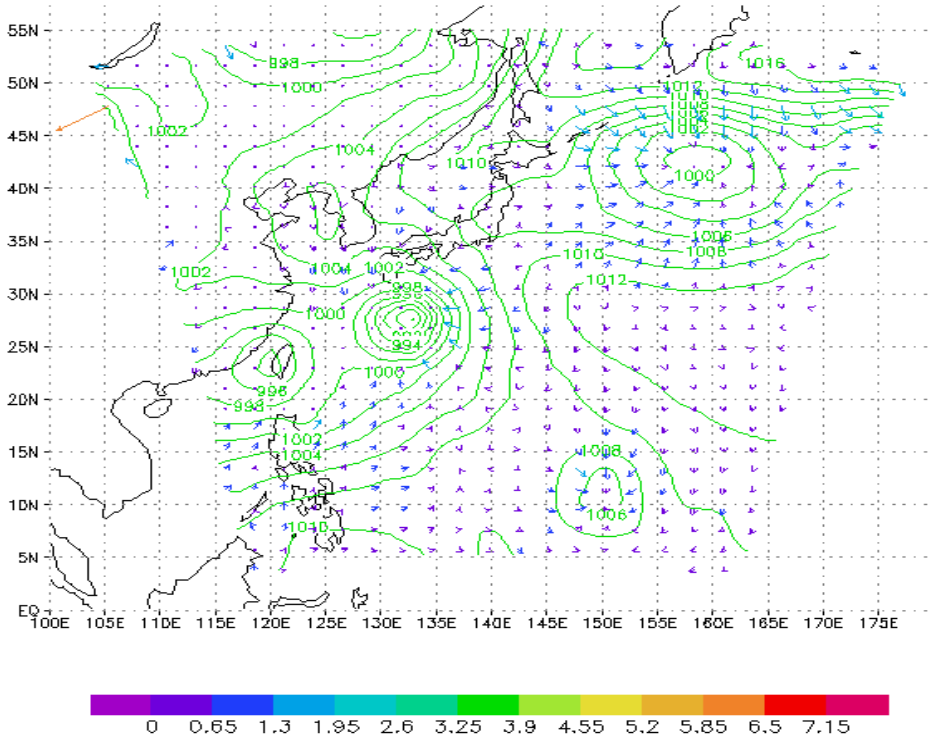

09.07.2002

b)

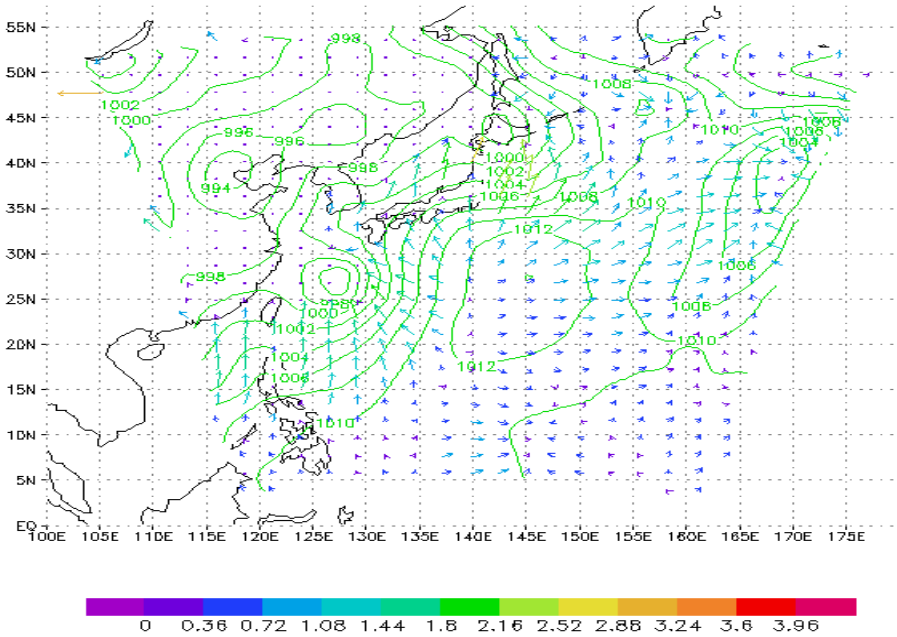

14.07.2002

Fig. 1a,b.

Study on limited-area short-range ensemble approaches targeted for heavy rain in Europe

Kai Sattler and Henrik Feddersen
Danish Meteorological Institute, Lyngbyvej 100, DK-2100 Copenhagen Ø
Email: ksa@dmi.dk

A common way to address the uncertainty in numerical weather prediction (NWP) is to design an ensemble, attempting to forecast the likelihood for the expected future event on basis of the best possible knowledge about the atmospheric state at the time of the forecast production. The interest of doing this with a high-resolution limited-area NWP model (LAM) has grown during the last years, and there are many different possibilities of designing a LAM ensemble. This study investigated two different approaches of creating a small LAM ensemble for rainfall prediction. They are both based on the Danish Meteorological Institute's (DMI) version of the HIgh Resolution Limited-Area Model DMI-HIRLAM, which has been configured as a doubly 1-way nested system, were the outer model receives initial as well as lateral boundary data from the ECMWF ensemble prediction system (EPS) in a 6 hour frequency. This outer model covers Europe and the North Atlantic as well as parts of North America. The inner DMI-HIRLAM model is the actual model of interest and covers Europe with a 0.1° grid. Integrations for this study were performed up to 72 hours ahead.

The first LAM ensemble is designed to represent an uncertainty in the initial condition (atmospheric state) as well as at the lateral LAM boundaries. It is created on basis of the ECMWF-EPS with 50+1 members, from which a small set of significant members is selected (selection ensemble (SE)). The significance of a member is estimated on basis of accumulated precipitation over the area of interest, which includes the river basin that may potentially experience flooding due to heavy rain. The control forecast is allways included in the selection. The selected members from the global EPS then make up the initial and boundary conditions for the members of this first LAM ensemble design. The size of the selection ensemble has been defined to be 5+1.

The second LAM ensemble tries to address model related uncertainty in the rainfall forecasts and consists of the variation of the physical representation of the condensation and convection processes within the LAM (parameterization ensemble (PE)). A similar approach has e. g. been investigated by Stensrud et al. (2000), even though with different schemes. Five parameterization schemes were available for this study:

- Stratiform condensation scheme (STC; Kållberg, 1989)
- Anthes-Kuo scheme (AKC; Kuo et al., 1974; Anthes, 1977)
- Sundquist scheme (SQS; Sundqvist, 1993)
- Tiedtke scheme (TDS; Tiedtke, 1993)
- STRACO (Sass et al., 1997)

This results in an ensemble size of 4+1, were the last member (STRACO) is identical with the control of the SE design.

The two ensemble designs SE and PE were tested on three historical heavy rain events in different European areas and of different synoptic and dynamic characteristics. The cases are the heavy rain over the Piemonte region in Northern Italy from November 1994, the strong precipitation during the end of January 1995 over the basins of the rivers Rhine and Meuse,

and the heavy rain over the Odra basin in Poland/Germany/Chzech Republic in July 1997. A validation using ranked histogramms shows that both designs exhibit too little ensemble spread (not shown), the PE designs, however, shows a larger spread than the SE. Reliability diagrams for the 5 mm threshold of 24 hour accumulated rainfall between 42–66 hours forecast range are shown in Fig. 1. The two ensemble designs perform comparably well, with the PE design tending to exhibit a slightly better reliability. Both designs generally tend to overestimate higher observation frequencies at this threshold.

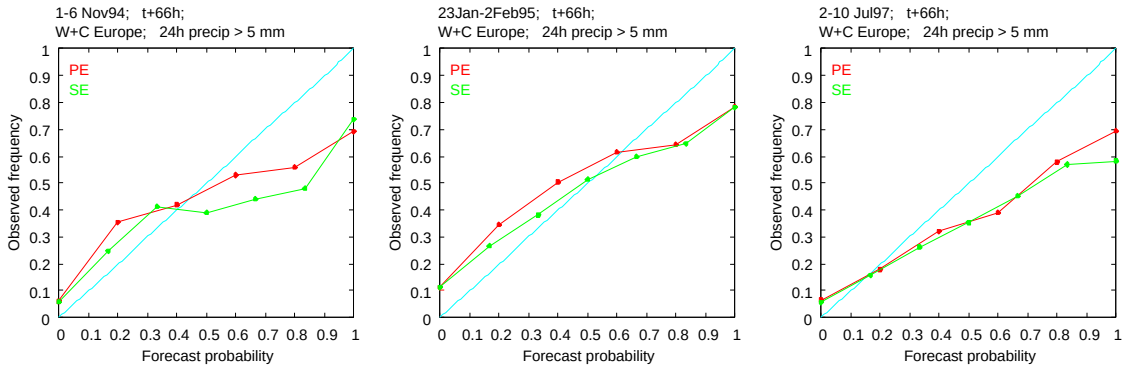

FIG. 1: Reliability diagrams for the 5 mm threshold of accumulated precipitation between 42–66 hours for the selection ensemble (green) and the parameterization ensemble (red), for the three cases of heavy rain: Piemonte case November 1994 (left), Rhine/Meuse case January 1995 (middle) and Odra case July 1997 (right).

The performance of the ensemble designs reveals to vary strongly from case to case and even on a daily basis, and a combination of both ensembles seems advantageous in many cases, but not in all. A weakness of the SE design is that the selection of the members is based on the global EPS rainfall fields only, because small scale effects as well as non-linear developments within the LAM integration are not known a priori. This may in some cases have the effect that the ensemble spread of the SE in the LAM rainfall is smaller compared to an ensemble integration of all 50+1 members with the LAM, even though this is the case in the global rainfall fields. The PE design is quite promising, as long as all schemes perform comparably well in order not to degrade the ensemble performance.

References

Anthes, R.A., 1977: A Cumulus Parameterization Scheme Utilizing a One-Dimensional Cloud Model. *Mon. Wea. Rev.*, **105**, 270–286.

Kuo, H.L., 1974: Further Studies of the Parameterization of the Influence of Cumulus Convection on Large-Scale Flow. *J. Atmos. Sci.*, **31**, 1232–1240.

Kållberg, P., 1989: *HIRLAM Forecast Model Level 1 Documentation Manual.* 77pp. Available from the Swedish Meteorological and Hydrological Institute (SMHI) Norrköping, Sweden.

Sass, B.H., 1997: Reduction of numerical noise connected to the parameterization of cloud and condensation processes in the HIRLAM model. *HIRLAM Newsletter*, **29**, 37–45. Available from the Swedish Meteorological and Hydrological Institute (SMHI) Norrköping, Sweden.

Stensrud, D.J., Bao, J.-W., Warner, T.T., 2000: Using initial condition and model physics perturbations in short-range ensembles. *Mon. Wea. Rev.*, **128**, 2077–2107.

Sundqvist, H., 1993: Inclusion of Ice Phase of Hydrometeors in Cloud Parameterization for Mesoscale and Large Scale Models. *Beitr. Phys. Atmos.*, **66**, 137–147.

Tiedtke, M., 1993: Representation of Clouds in Large-Scale Models. *Mon. Wea. Rev.*, **121**, 3040–3061.

NUMERICAL STUDY OF THE SHAPES AND MAINTENANCE MECHANISMS OF MESO-β SCALE LINE-SHAPED PRECIPITATION SYSTEM IN THE MIDDLE-LATITUDES

Hiromu Seko[(1)], Hajime Nakamura[(2)]

[(1)] Meteorological Research Institute, Japan Meteorological Agency, Tsukuba, Japan
[(2)] Numerical Prediction Division, Japan Meteorological Agency, Tokyo, Japan

1. Introduction

Precipitation systems that cause severe disasters often have the line-shaped precipitation regions. These precipitation system has a scale of 100km (meso-β scale), and the convective cells generate one after another in the systems. The repeating generation of the cells leads to the long life of the systems.

Line-shaped precipitation systems reported so far are divided into mainly two types; squall line (SL) type and back building (BB) type. The structure of the SL type is similar to the squall lines observed in the Midwest of U.S. In the BB system, the convective cells generate in the tip of the system repeatedly, and move backward. Besides these types, the systems with the carrot-shaped cloud region often inflict heavy rainfalls.

The structure and long-lasting mechanism of the SL type are relatively well-known. However, other types are not fully investigated yet. Therefore, the precipitation systems of each type were analyzed by special observation data and the outputs of the numerical simulation. The results of the analyses are summarized in the section 2.

Because the results of the analyses indicate that the environment of the systems (e.g. vertical profiles of horizontal wind and humidity) depends on their types, the numerical experiments were performed by changing the environment conditions to investigate the factors that determine the type of the precipitation systems.

2. Case studies

In this section, the observed features of the observed line-shaped precipitation systems are summarized.

2.1 Squall line (SL) type

A line-shaped precipitation system developed over the Kanto area on 16 August 1995 (Seko et al,1998). The intense convections developed along the front side of the system, and the wide weak precipitation region existed on its rear side. The airflow structure consisted of the two airflows: One is the low-level inflow of warm and humid air from the south. It was lifted up by the outflow of the system along its front-side edge. And another flow is the middle-level rear inflow that invaded into the system. When this system passed, the temperature descended more than 10°C and the gust of 24m/s was observed. This indicates that the rear inflow generated the cold pool by the evaporation of the water substances.

2.2 Back Building (BB) type

The cloud cluster that consisted of the several meso-βscale precipitation systems stayed over the southern Kyushu on 7 July 1996 (Seko et al. 2000). The meso-β scale system was further composed of several short convective bands. The short band in the meso-β scale system indicates that a scale exists between the meso-β scale and meso-γ scale. Hereinafter, this scale of the short bands is referred to as the meso-βs scale. In these meso-βs bands, the new convective cells generate at the tip of the band repeatedly, and moved backward. Because the generation point of the cells was only near the tip of the band, the length of the bands was shorter than that of the meso-β scale system. The direction of the middle-level inflow was almost same to that of the low-level inflow, and the bands extended to the leeward side of the middle-level wind. The low-level inflows entered the meso-β system from the south and ascended at the tip of the meso-βs scale bands. The middle-level airflows passed between the meso-βs scale bands.

2.3 Back and Side Building (BSB) type

The precipitation system with the carrot shaped cloud region was observed over the Kanto area when the typhoon 9426 was approaching to Japan (Seko et al.1999). The precipitation system extended to the same direction of the middle-level wind and the width of the cloud became wider at the leeward side, producing the carrot-shaped cloud region. The relation of the low-level inflow and middle-level wind was different from those of the SL type and the BB type: the direction of the middle-wind was perpendicular to that of the low-level inflow. The convective cells were generated on the upwind side of the middle-level wind (back building) and moved to the leeward side, and merged into the long intense convective band. After merging with the band, the convective cell was enhanced by the low-level inflow from its lateral side (side building). From these features, this carrot-shaped band had the new mechanism that should be called 'back and side building type'.

3. Numerical experiment under the simplified environmental condition

The comparison of the observed precipitation systems suggests the environmental factors that determine their type. The low-level convergence was common in aforementioned three cases. On the other hand, the middle-level wind direction to the low-level inflow and the middle-level humidity depended on the types. Thus, the numerical simulations were performed by changing these factors. In this study, non-hydrostatic model of Meteorological Research Institute was used. The horizontal grid interval of 2km was adapted to reproduce the convective cells.

When the direction of the middle-level wind was opposite to that of the low-level inflow, the intense convective band developed along the convergence line. The rear inflow at the middle-level descended and the cold pool was produced near the surface (Fig. 1a).

When the directions of the middle-level wind was same as that of the low-level inflow, the short convective bands generated side by side along the convergence line in the meso-β scale system (Fig. 1b). The short convective bands extended to the direction of the middle-level wind. In these bands, the new convective cells were generated at the upwind tip of the bands, and moved to leeward. When the direction of the middle-level wind was perpendicular to the low-level inflow, the intense band developed (Fig. 1c).

*Corresponding author address: Hiromu Seko
Meteorological Research Institute,
1-1, Nagamine, Tsukuba, Ibaraki, 305-0052, Japan,
e-mail:hseko@mri-jma.go.jp

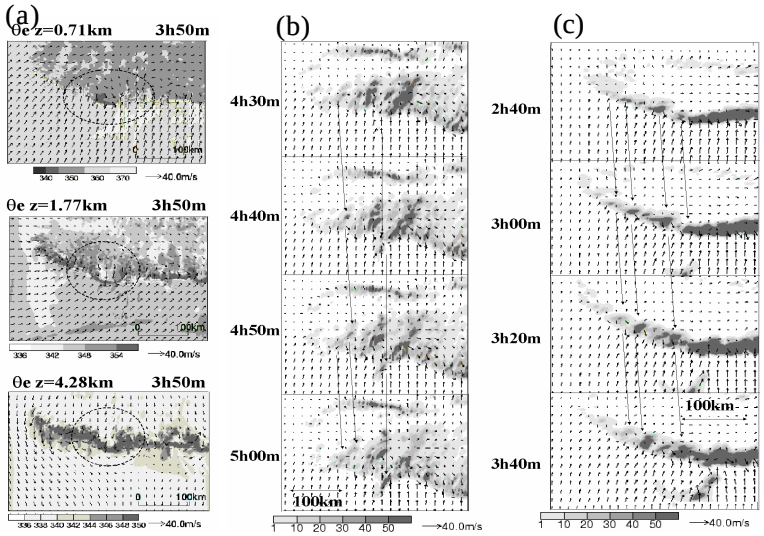

Fig.1 Precipitation system simulated with the simplified environment condition. (a) Horizontal distribution of equivalent potential temperature when the middle-level wind direction is opposite to the low-level inflow. (b)Precipitation distribution when the directions of the middle-level wind and low-level inflow are same. (c) Same as (b) except for the middle-level direction perpendicular to the low-level inflow.

Although the shape of the band was similar to the band in which the direction of the middle-level wind was opposite to that of the low-level inflow, the middle-level airflow did not descend and the intense cold pool was not produced. The convective cells generated on the upwind side of the middle-level flow, and moved to leeward.

These simulated features in three experiments were the same as the observed ones. This result indicates that the direction of the middle-level wind is one of factors that determine the type of the precipitation system.

When the relative humidity between the heights of 1.5km and 4.5km was reduced, the relation between the type of the precipitation systems and the directions of the middle-level wind and low-level inflow was not changed, although the weak precipitation generated more widely. This result indicates that the middle-level humidity is not the primary factor that determines the type of the system.

4. SUMMARY

Besides the precipitation systems of the SL type and the BB type that have been investigated so far, it was found that the precipitation system of the BSB type that often caused the heavy rainfall exists.

When three types of the precipitation bands were compared, there are the differences in their environments and structures. As for the environment of the systems, when the direction of the middle-level wind is opposite, same and perpendicular to that of the low-level inflow, the precipitation system of the SL type, the BB type and the BSB type developed.

The shapes and structures of these systems were explained from the viewpoint of the middle-level wind (Fig.2). In the SL, the middle-level rear wind descends in the precipitation system and enhances the outflow of cold air. The outflow intensifies the convergence with the low-level inflow, and the narrow intense convective band developed along the convergence line. In the BB type, the middle-level wind moves the convective cells to leeward, producing the meso-βs scale convective bands. Since the directions of the low-level and middle-level winds are same, the structure, with which the meso-βs scale bands develop side by side, is favorable for the low-level inflow to ascend without disturbing the middle-level wind. In BSB type, the new cell generates on the upwind side of the band, and moves to leeward with being intensified by the low-level inflow from the lateral side. This evolution of the cells produces the carrot-shaped precipitation region.

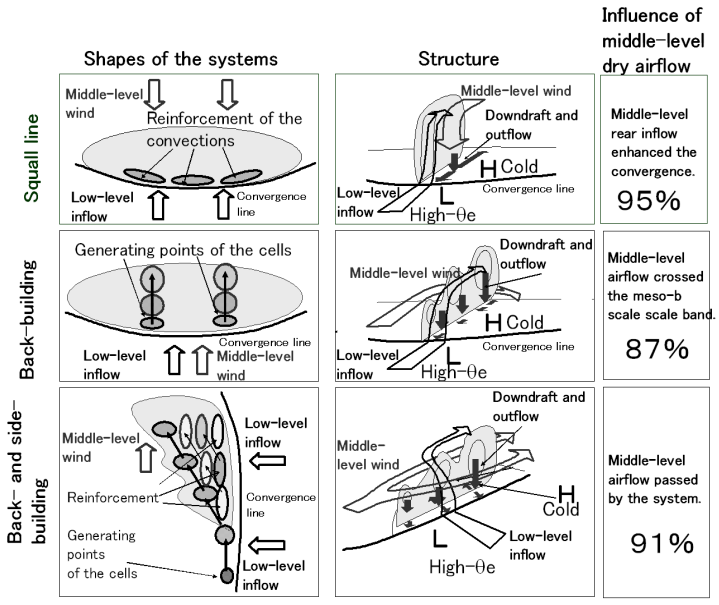

Fig.2 Schematic illustration of the shapes and structures of the precipitation systems. Right column indicates the decrease rate of precipitation amount

The numerical experiments were also performed with changing the middle-level humidity. The types of the systems were not changed when the middle-level humidity was reduced. However, the decrease of precipitation amount depends on the types. Precipitation amount was decreased slightly in the SL type, while it was decreased significantly in the BB type. This difference can be explained by the middle-revel flow. In the BB type, the middle-level flows entered the meso-β scale precipitation system and evaporated water substances while they crossed the precipitation regions. In the BSB type, the middle-level flow made a detour to avoid the system and the middle-level airflow did not evaporate water substances of the system. In the SL type, the cool pool that was intensified by the middle-level rear inflow strengthened the low-level convergence, enhancing the convections, although the rear inflow evaporated water substances.

Model of real classification of meteorological parameters for regional prognosis

S. Senotrusova, V. Svinuhov*

Far Eastern State University

30-61 Aleutskaya St., 690000 Vladivostok, Russia
E-mail:svetlsen@mail.ru

Offered model of short-term regional prognosis. The main idea of the method is to pick out air mass of area investigation, using common meteorological variable and synoptical parameters. Thus, initial point of offered method is the classification of air mass. Certain limits are put on meteorological variable quantity. Firstly, they are to be all to distinguish will air mass and, at the same time, they are to change a little within air mass itself. Secondly, they are to be regularly observed by variable quantities in the net of the stations.

Presently initial information is usually given as a set of quantitative (numerical) indications. When transforming of initial information is the method of main components often used, which is will known in the meteorology as the method of decomposition into natural orthogonal components [1]. Decomposition of fields according to space is usually given. In contrast to that method in this paper decomposition was given according to time [1,2]. Fulfilling this work the data of aerological station “Sad-gorod” (Garden-City) and table TM-1 meteostation in Vladivostok (Primorie Territory) within 1975-1995 were used. Analysing these findings many factors were under consideration. Such as: direction and speed wind, temperature and air humidity, pressure, temperature of dew-point on the mixing surface level, and speed of wind, temperature air humidity, pressure above 500-1500 meters sea-level. According to aerological station height of air layer shift was counted average daily. As a parameter showing vertical atmosphere steadiness difference altitude temperature and the temperature 500 ms above surface of earth. Thus, matrix of meteorological parameters and synoptical variable quantities measured by 20*174 was used. Decomposition of variable quantities into natural orthogonal functions selected eleven components, describing 86 per cent of variable dispersion for cold season and 82 per sent for warm season. Coefficient of decomposition matrix results (measured 11*174) may be classified in groups by different methods. And finally, statistic method of objective classification was used in this work as well for revealing homogeneous local groups in certain point totality of multi-measured sign space. The task was being solved with the help of criteria searching, finding of it gave the possibility to evaluate the homogeneity of totality under consideration. Analogy criterion by Pirson was used in this work for classify of succession of variable quantities. Classify decomposition coefficients according to this method let us receive ten groups for cold half year and 12 groups for warm six months. Every of these groups can be characterized by the particularities of general circulation and complex of meteorological parameters. Mean quantity of meteorological variable quantities (such as: direction and wind speed, pressure, temperature, air humidity on the level of stretching surface, temperature, wind speed, pressure and air humidity on the level 500 meters and 1,5 km above earth surface and others) were counted for each group. Moreover, every group was depicted by typical synoptical situation let’s take an example of a few typical synoptical situation describing. Let’s describe a few typical synoptical situations as an example. Synoptical situation in the South region of Primorie Territory for the first group is determined by south cyclone. Trajectory of centre cyclone displacement passes from Yellow Sea region along Japanese Islands. South regions of Primorsky Territory are under influence of the North originally and then North-West

periphery of cyclone. As a result, we could observe relative low temperatures (-11C, -15C) in the investigated region. 10-15 m/sec speed North-East and North-Wind mainly. Sea air masses of temperate latitudes dominate over the South of Primoriye. The other group is characterized by intensive cyclonic activity over Far-Eastern Seas. This is a crest of Asian anticyclone over Primorye. Thus, each group had the following characteristics: typical air masses, meteorological parameters and certain synoptical situation. This approach may be useful for pollution prognosis in the close land air mass and population morbidity in the industrial city prognosis. Analysis give the possibility to pick out classters (and consequently, groups of synoptical situations and meteorological parameters) which greatly determine the high level atmosphere pollution and therefore the morbidity of population. Our investigation shows that in winter 3 synoptical situations from 10 being under study has high potential of atmosphere pollution. Low height of mixing atmosphere layer in the morning 70 meters, low wind speed at the earth surface (3,5m/s),little displacement of wind speed in the close land layer 3,5 m/s and 7,4 m/s) high background of temperature at the earth surface (-3,8 C) are the typical characteristics situation for these groups. Taking the second step, prognosis of a certain synoptical group gives the possibility to expand the results of out investigation for prognostic some meteorological components, potential of atmosphere pollution and population morbidity, using equation of step by step regression or discriminant analyses. To solve the second and the third tasks for building prognosis equation it is necessary to use the information on the atmosphere pollution and population morbidity in the cities.

This approach is very effective for getting good results, which are impossible to receive under traditional methods.

They are:

To identify specific synoptical situations and air mass, describe typical potential of air pollution for these synoptical situations;

To pick out the groups of dominating air mass, where the potential of pollution especially high;

To identify the groups of parameters, characterizing the conditions of low and high potential of atmosphere pollution;

To determine groups parameters, describing conditions of appearing close earth and slightly lifted inversion.

RFERENCES

1. Danltrey S. Principal components analisis. Concept and technigues in Modern Geography. 1976,8/1.-51p.
2. Warld J. Hierarchical grouping to optimize an objective function// J.Amer.Statistic.Ass., 1963,58,pp.236-244.

Ensemble Forecasting of Tropical Cyclone Motion Using A Baroclinic Model

Xiaqiong Zhou[1] [2]and Johnny C L Chan [2]

[1] *Shanghai Typhoon Institute, China Meteorological Administration*
[2]*Laboratory for Atmospheric Research, Department of Physics and Materials Science*
City University of Hong Kong (email: johnny.chan@cityu.edu.hk)

1. Introduction

While some studies have been conducted in the ensemble forecasting (EF) of tropical cyclone (TC) motion (Aberson et al. 1995, 1998; Cheung and Chan 1999a, b, hereafter CCa and CCb respectively; Cheung 2001), much more efforts are needed to establish EF as a viable alternative to the traditional single solution from a numerical-weather-prediction model for TC motion forecast.

In this paper, the lagged-averaged forecast (LAF) and regional breeding of growing modes (BGM) perturbation methods are applied to the baroclinic model of the University of New South Wales (Leslie et al. 1985) to estimate the effectiveness of these EF techniques in TC motion forecast. Five cases from three typhoons that occurred during the Tropical Cyclone Motion Experiment (TCM-90) are chosen for study.

2. Model and data

The model is a hydrostatic primitive equation model with a horizontal grid spacing of 30 km and 24 internal vertical sigma levels. The modified Kuo and Kain-Fritsch cumulus parameterization schemes are used. The initial fields are taken from the TCM-90 dataset. The bogussing scheme of the Typhoon Model (TYM) of the Japan Meteorological Agency is used in some of experiments after filtering the analysis vortex. Forecast time is up to 72 h.

The LAF perturbations are generated from the differences between the short-range forecasts. No vortex-environment flow separation is applied (Cheung 2001). The BGM perturbation scheme is similar to that of CCa, CCb. When employing the BGM technique, TC vortex–environment separation is applied (BGMV and BGME respectively). Six pairs of ensemble members are generated in all three methods: LAF, BGMV and BGME.

3. Forecast results

a. Typhoon Yancy

Typhoon Yancy of 1990 at the initial time of 00UTC 17 August (to be labeled as Y1700) is chosen as an example. In all three sets of experiments no bogus scheme is included because the analysis vortex seems to be well represented by the TYM-90 analysis. Most of the LAF members predicted the landfall of Yancy over Taiwan except one that passed to its north as the control (Fig. 1). Two of the landfall members showed a jump across the Central Mountain Range. The ensemble mean track is much closer to the best track than that in the control run. In the BGME and BGMV experiments, the mean forecast tracks also show an improvement over the control though landfall is not predicted (not shown).

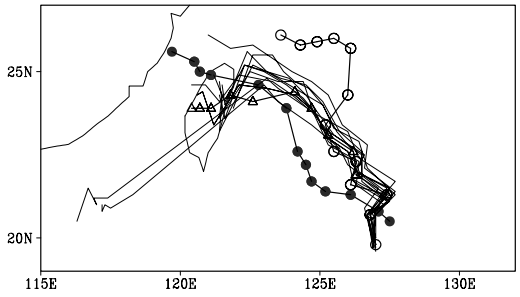

Fig. 1. Ensemble tracks (thin lines) of Yancy (Y1700) using the LAF technique. Best track – closed circle, control - open circle, ensemble mean – triangle. Positions are plotted every 6 h.

b. Ed and Flo

1) SENSITIVITY EXPERIMENTS

The forecast track of Ed turns towards the south instead of a steady westward movement, resulting in a 1000-km position error by 72 h (Fig. 2). Possible factors contributing to the failure of the forecasts of Ed such as cumulus parameterization,

bogussing scheme and lateral boundary, the influences of Flo and subtropical ridge are examined from 00UTC 14 September 1990 and 00UTC 15 September 1990 (to be labeled as E1400 and E1500 for the Ed, and F1400 and F1500 for the Flo respectively).

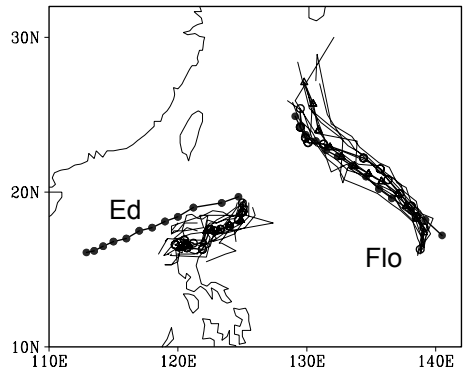

Fig. 2. As Fig. 1 except for Ed and Flo (E1400, F1400).

The tracks of Ed are surprisingly insensitive to the possible factors (not shown). The forecast errors of the environment, which includes the subtropical ridge and the outer flow of Flo, largely contribute to forecast failure of the movement of Ed. The weakening subtropical ridge over the South China is replaced by a continuously deepening trough. The northwesterly flow upstream of the westerly trough pushes Ed to the southeast. At the same time, the outer flows of Ed and Flo merge due to the lack of the interference of the subtropical ridge. When Flo moves to the northeast of Ed, the outer flow of Flo makes Ed accelerate and move to the southeast.

2) ENSEMBLE FORECASTS OF FLO AND ED

The three EF techniques are performed on the cases of Ed and Flo. For Ed, no significant improvement is obtained because the forecast of the western part of the subtropical ridge is not improved when the analysis is perturbed by the LAF errors (Fig. 2). For F1400, the control run performs well, and the position errors remain below 100 km from 48 to 72 h. The mean track is close to the best track except that it has a larger movement speed.

Bogussing scheme is used in the BGMV and BGME experiments. In the EF experiments of Ed, although some members have more westward movement when the vortex or the environment is perturbed, the evolution of the environment in EF forecasts is not improved apparently. The ensemble mean is similar to that of the control.

The forecast errors come not only from the errors of the initial state also from the model. According to the results of the sensitivity experiments and the EF experiments, the main problem in this study is the large forecast errors of Ed. The model cannot predict the evolution of the subtropical ridge correctly in any of experiments. It appears that the forecasts moved along with a certain attractor of the model.

References:

Aberson, S. D., S. J. Lord, M. DeMaria, and M. S. Tracton, 1995: Short-range ensemble forecasting of hurricane tracks. *21st Conf. Hurr. Trop. Meteor., Miami*, Amer. Meteor. Soc., 494-497.

Aberson, S. D., M. A. Bender, and R. E. Tuleya, 1998: Ensemble forecasting of tropical cyclone tracks. *12th Conf. Num. Wea. Pred., Phoenix*, Amer. Meteor. Soc., 290-292.

Cheung, K. K. W., 2001: Ensemble forecasting of tropical cyclone motion: comparison between regional bred modes and random perturbations. *Meteor. Atmos. Phys.,* **78,** 23-34.

Cheung, K. K. W. and J. C. L Chan, 1999a: Ensemble forecasting of tropical cyclone motion using a barotropic model. Part I: Perturbations for the environment. *Mon. Wea. Rev*. **127**, 1229-1243.

Cheung, K. K. W. and J. C. L Chan, 1999b: Ensemble forecasting of tropical cyclone motion using a barotropic model. Part II: Perturbations of vortex. *Mon. Wea. Rev*., **127**, 2617-2640.

Leslie, L. M., G. A. Mills, L. Logan, D. J. Gauntlett, G. A. Kelly, M. J. Manton, J. McGregor, and J. Sardie, 1985: A high resolution primitive equations NWP model for operations and research. *Aust. Met. Mag.,* **33**, 11-35.